

TALLINN UNIVERSITY OF TECHNOLOGY  
School of Information Technologies

NAFISAT GYIMAH  
184597IVEM

**PARAMETRIC ANALYSIS AND  
OPTIMIZATION OF AIN-BASED RF MEMS  
SWITCHES.**

Master's Thesis

Supervisor: Mehadi Hasan Ziko (Ph.D.)

Co. Supervisor: Ants Koel (Assoc. Professor)

Tallinn 2020

TALLINNA TEHNIKAÜLIKOOL  
Infotehnoloogia teaduskond

NAFISAT GYIMAH  
184597IVEM

**ALUMIINIUMNITRIIDIL (AIN)  
PÕHINEVATE RAADIOSAGEDUSLIKE  
MIKROELEKTROMEHAANILISTE (MEMS)  
LÜLITITE PARAMEETRILINE ANALÜÜS  
JA OPTIMEERIMINE.**

Magistritöö

Juhendaja: Mehadi Hasan Ziko (Doktorikraad)

Kaasjuhendaja: Ants Koel (Seostada Professor)

Tallinn 2020

## **Author's declaration of originality**

I hereby certify that I am the sole author of this thesis. All the used materials, references to the literature, and the work of others have been referred. This thesis has not been presented for examination anywhere else.

Author: Nafisat Gyimah

20.04.2020

## Abstract

RF MEMS switches exhibit excellent performance at high frequencies in comparison to semiconductor devices. The technology of MEMS switches using the electrostatic principle has been extensively developed. Unfortunately, practical difficulties, such as high actuation voltage, and poor power handling, have proven hard to resolve, and the wider adoption of these devices has been delayed. This thesis explores the possibility of achieving low actuation voltage and high contact force with Aluminium Nitride (AlN)-based piezoelectric RF MEMS switches. A comprehensive model for the mechanical and electrical behaviour of the switch is analyzed to obtain an optimized design of a high-performance switch by analysing the effects of the geometry, structure, materials, and applied voltage. The mathematical (MATLAB) models are used preliminary to obtain the optimized geometrical design parameters. Results from mathematical models were compared with the Finite Element Model (FEM) analysis using the commercial COMSOL Multiphysics FEM. From the optimization analysis, an actuation voltage of 7V for a single beam and 5V for the dual-beam is obtained. The contact force of  $0.009\mu\text{N}$  in the single beam and  $0.9\mu\text{N}$  in a dual-beam is achieved. Furthermore, the single beam and dual beam RF MEMS switches show resonance frequencies are 3.5MHz and 1.32MHz respectively.

## Annotatsioon

RF MEMS lülitid on pooljuhtseadmetega suurepärased kõrgetel sagedustel. Elektrostaatiliselt põhimõtet kasutavate MEMS-lülitite tehnoloogiat on laialdaselt arendatud. Kahjuks on praktilisi probleeme, nagu kõrge käivituspinge ja kehv energiakäsitlus, lahendada raskesti ning nende seadmete laiem kasutuselevõtt on viibinud. See lõputöö uurib võimalust saavutada alumiiniumnitriidil (AlN) põhinevate piezoelektriliste RF MEMS-lülititega madal käivituspinge ja suur kontaktjõud. Analüüsitakse lüliti mehaanilise ja elektrilise käitumise terviklikku mudelit, et saada suure jõudlusega lüliti optimeeritud kujundus, analüüsides geomeetria, struktuuri, materjalide ja rakendatava pinge mõju. Matemaatilisi (MATLAB) mudeleid kasutatakse optimeeritud geomeetriliste kujundusparameetrite saamiseks esialgu. Matemaatiliste mudelite tulemusi võrreldi lõplike elementide mudeli (FEM) analüüsiga, kasutades kommertslikku COMSOL Multiphysics FEM. Optimeerimisanalüüsist saadakse ühe tala jaoks 7V ja topeltkiire puhul 5V akupinge. Saavutatakse kontaktjõud 0,009  $\mu\text{N}$  ühe valgusvihu ja 0,9  $\mu\text{N}$  kahe valgusvihu korral. Lisaks näitavad ühe- ja kahekiireliste RF MEMS-lülitite resonantssagedused vastavalt 3,5MHz ja 1,32MHz

## List of abbreviations and terms

AlN	Aluminium Nitride
Au	Gold
CMOS	Complementary metal-oxide-semiconductor
CSMB	Capacitive-Silicon bulk micromachining
DC	Direct Current
EETAsia	EE Times Asia
E <sub>g</sub>	Band gap
GaAs	Gallium Arsenide
FBAR	Film bulk acoustic resonators
FEM	Finite Element Modeling
FET	Field Effect Transistor
LiNbO <sub>3</sub>	Lithium Niobite
MEMS	Micro Electromechanical Switches
pHEMT	Pseudomorphic High Electron Mobility Transistor
PZT	Lead Zirconate Titanite
RF	Radio Frequency
RSBM	Resistive-Silicon bulk micromachining
Si	Silicon
SiC	Silicon Carbide
SIO	Silicon on insulator
SiO <sub>2</sub>	Silicon dioxide
V <sub>ON</sub>	Threshold Voltage
WLFT	Wafer level transfer technologies
ZnO	Zinc Oxide

## Table of contents

Author's declaration of originality .....	3
Abstract.....	4
Annotatsioon.....	5
List of abbreviations and terms .....	6
Table of contents .....	7
List of figures .....	9
List of tables .....	11
1 Introduction .....	12
1.1 Basics and classification of RF MEMS switches .....	12
1.2 Performance of RF MEMS switches .....	13
1.3 Benefits and application areas of RF MEMS switches .....	13
1.4 Motivation .....	14
1.5 Research objectives .....	15
1.6 Structure of the thesis .....	16
2 Overview of piezoelectric materials .....	17
2.1 Piezoelectric RF Mems Switches - State of the Art .....	18
3 Modelling of RF MEMS switch .....	22
3.1 Theory governing the mathematical model .....	23
3.2 Structure of the piezoelectric cantilever beam model .....	23
3.3 Mathematical modelling of displacement.....	24
3.4 MATLAB simulations.....	26
3.4.1 Beam deflection analysis .....	27
3.4.2 Effect of piezoelectric thickness.....	27
3.4.3 Effect of substrate thickness .....	28
3.4.4 Effect of beam width .....	29
3.4.5 Effect of actuation voltage.....	30
3.5 Mathematical modelling of actuation voltage .....	30
3.6 Mathematical modelling of contact force.....	33
3.7 MATLAB simulations .....	34

3.7.1 Effect of switch gap.....	34
3.7.2 Effect of beam length and width .....	35
3.7.3 Effect of piezoelectric thickness.....	37
3.7.4 Effect of actuation voltage.....	37
4 Finite element modelling of RF MEM switches .....	39
4.1 RF MEMS switch structures used in COMSOL .....	39
4.2 Material properties.....	41
4.3 Simulation setup .....	42
4.4 3D Model results obtained.....	42
4.5 Deflection analysis .....	44
4.5.1 Comparative analysis for varying beam length .....	44
4.5.2 Comparative analysis for varying beam width.....	46
4.5.3 Comparative analysis for varying piezoelectric thickness .....	47
4.5.4 Comparative analysis for varying substrate thickness.....	48
4.6 Contact force analysis.....	50
4.7 Eigenfrequency analysis .....	51
4.7.1 Comparative analysis for varying beam length .....	52
4.7.2 Comparative analysis for varying beam width.....	53
4.7.3 Comparative analysis for varying substrate thickness.....	53
4.7.4 Comparative analysis for varying piezoelectric thickness .....	54
4.7.5 Comparative analysis for varying applied voltage .....	54
5 Optimisation .....	56
6 Summary.....	60
References .....	61



## List of figures

Figure 1. 2017-2022 MEMS market forecast-In US\$B (Yole Développement, May 2017) [12]. .....	14
Figure 2. Total MEMS market by a. Device b. Application [13].....	15
Figure 3. Flowchart for modelling RF MEMS Switch.....	22
Figure 4. Euler-Bernoulli Beam Theory Assumptions: The plane section remains normal to the axis of the beam after deformation [37] .....	23
Figure 5. Piezoelectric cantilever beam model.....	24
Figure 6. Deflection of Piezoelectric switch in response to applied voltage.....	24
Figure 7. Displacements versus beam length for varying piezoelectric thickness .....	28
Figure 8. Displacement versus beam length for varying substrate thickness .....	29
Figure 9. Displacement versus beam length for varying beam width .....	29
Figure 10. Displacement versus beam length for varying actuation voltage.....	30
Figure 11. Displacements versus actuation voltage for varying beam length.....	32
Figure 12 Displacements versus beam length for varying piezoelectric coefficient.....	32
Figure 13. Contact force acting at switch contact region [41] .....	33
Figure 14. Contact force versus beam length for varying switch gap .....	35
Figure 15. Contact force versus substrate thickness for varying length.....	36
Figure 16 Contact force versus substrate thickness for varying beam width .....	36
Figure 17. Contact force versus substrate thickness for varying Piezoelectric thickness .....	37
Figure 18. Contact force versus actuation voltage .....	37
Figure 19. Modelling process steps for RF MEMS switch in COMSOL .....	39
Figure 20. Proposed cantilever designs used in FEM analysis.....	41
Figure 21. 3D model for displacement field and stress distribution.....	44
Figure 22. Displacement versus beam length plot for single beam.....	45
Figure 23. Displacement versus beam length for the four geometries .....	45
Figure 24. Displacement versus beam width for single beam.....	46
Figure 25. Displacement versus beam width plot for the four geometries.....	46
Figure 26. Displacement versus beam piezoelectric thickness for single beam.....	47

Figure 27. Displacement versus beam piezoelectric thickness for the four geometries.	48
Figure 28. Displacement versus beam substrate thickness for single beam.....	49
Figure 29. Displacement versus beam substrate thickness plot for the four geometries	49
Figure 30. 3D for contact figure pressure.....	51
Figure 31. 3D for Eigen frequency mode shapes .....	52
Figure 32. Eigen frequency versus beam length for the four geometries.....	52
Figure 33. Eigen frequency versus beam width for the four geometries.....	53
Figure 34. Eigen frequency versus substrate thickness for the four geometries .....	54
Figure 35. Eigen frequency versus piezoelectric thickness for the four geometries .....	54
Figure 36. Eigen frequency versus applied voltage for the four geometries.....	55
Figure 37. Displacement versus voltage for optimized geometry (Single Beam).....	58
Figure 38. Displacement versus voltage for optimized geometry (All four geometries)	58
Figure 39. Contact force vs actuation voltage for single beam .....	59
Figure 40. Contact force vs actuation voltage for dual beams with contact.....	59

## List of tables

Table 1. Comparison of RF MEMS, PIN Diode and FETs switches [5] .....	13
Table 2 Properties of piezoelectric materials: PZT, LiNbO <sub>3</sub> , AlN and ZnO [19] .....	17
Table 3 State of the art of piezoelectric RF MEMS switches .....	19
Table 4 Geometry and material properties of the proposed switch model .....	27
Table 5 Order of simulations for displacement analysis .....	27
Table 6 Order of simulations for contact force analysis.....	34
Table 7 Material properties and dimensions.....	41
Table 8 Comparison of displacement for different geometry at 5V.....	50

# 1 Introduction

Micro-Electro-Mechanical Systems (MEMS) technology is the miniaturization of mechanical and electro-mechanical devices and structures, using microfabrication techniques. A critical property of MEMS devices is their size, which varies from below one micron to several millimetres. As a result of MEMS technology, the integration of several micro-components on a single chip to form a microsystem that can sense and control an environment is realized [1]. In the last decade, devices such as switches, voltage-driven capacitors, inductors, acoustic and mechanical resonators, all employing MEMS technology, have experienced tremendous growth, particularly in radio frequency (RF) applications. Among these devices, RF MEMS switches are one of the most fundamental and important MEMS devices in the RF/microwave field and can also be incorporated into other RF MEMS devices [2][3].

## 1.1 Basics and classification of RF MEMS switches

RF MEMS switches are devices included in transmission line designs in order to achieve a closed or an open circuit. RF MEMS switches operate at RF to mm/wave (0.1-100GHz) [4]. An RF MEMS Switch has two main sections; the electrical section and the mechanical section. The mechanical section, which is responsible for the movement of the switch to the ON or OFF state, can be controlled by four different actuation principles: electrostatic, electromagnetic, piezoelectric or thermal. Amongst these, magnetostatic and thermal actuation provide high-contact force and low-actuation voltage, but longer switch time and greater power consumption, whilst piezoelectric actuation exhibits fast switch time and low-actuation voltage [5]. Furthermore, research has been carried out exploring the combination of two mechanisms, such as the combination of magnetostatic and electrostatic mechanisms [6], electrostatic and piezoelectric mechanisms [7], and thermal and electrostatic mechanisms [8], towards reducing the actuation voltage. Besides, the switch layout determines whether it moves horizontally or vertically.

The electrical section can be either series- or shunt-configured and can have metal-to-metal or a capacitive contact type. The metal-to-metal contact type (for both series and shunt configurations) has low insertion and isolation losses for DC to the Gigahertz (GHz) frequency range, with isolation loss largely due to parasitic capacitance, and insertion loss arising from contact resistance. Capacitive series switches and capacitive shunt switches experience low losses, in the 1-10GHz and tens of GHz frequency range, respectively. Generally, capacitive shunt RF MEM switches are most popular, due to their excellent performance at high frequencies [9, 10]. Altogether, there can be at least 32 types of RF MEMS Switch designs, using combinations of actuation methods, contact type, and circuit configuration [5].

## **1.2 Performance of RF MEMS switches**

RF MEMS switches have both mechanical and semiconductor properties and advantages. These switches exhibit excellent RF performance and low direct current (DC) power consumption. RF MEMS switches operate at high radio frequency range of 20THz to 80THz, while PIN Diodes and FETs operate at frequency ranges of 1 THz to 4 THz and 0.5 THz to 2 THz respectively [5]. In addition, RF MEMS switches offer low insertion loss (0.1 dB) and high isolation (>40 dB) at 1 GHz [1]. The superior performance of RF MEMS switches in comparison with conventional semiconductor switches, such as GaAs (Gallium Arsenide)-based FET (Field Effect Transistor), PHEMT (Pseudomorphic High Electron Mobility Transistor) or PIN-diode switches, has created much interest in their research and development.

## **1.3 Benefits and application areas of RF MEMS switches**

RF MEMS switches have the prospects of becoming more popular than traditional semiconductor and mechanical switches for wireless applications [3]. The key application areas of RF MEMS switches are as follows [11]:

- a) High-value applications – satellites, military tactical radio, military phased array
- b) Test equipment – RF instrumentation, automated test equipment (ATE)
- c) Telecommunication infrastructure – base stations, microwave communications
- d) Mass applications – mobile phones, consumer electronics, and IT

## 1.4 Motivation

The Global RF MEMS Market is expected to grow at a CAGR (compound annual growth rate) of approximately 35% by the year 2022, according to a market survey published in 2017 [12], as shown in Figure 1.

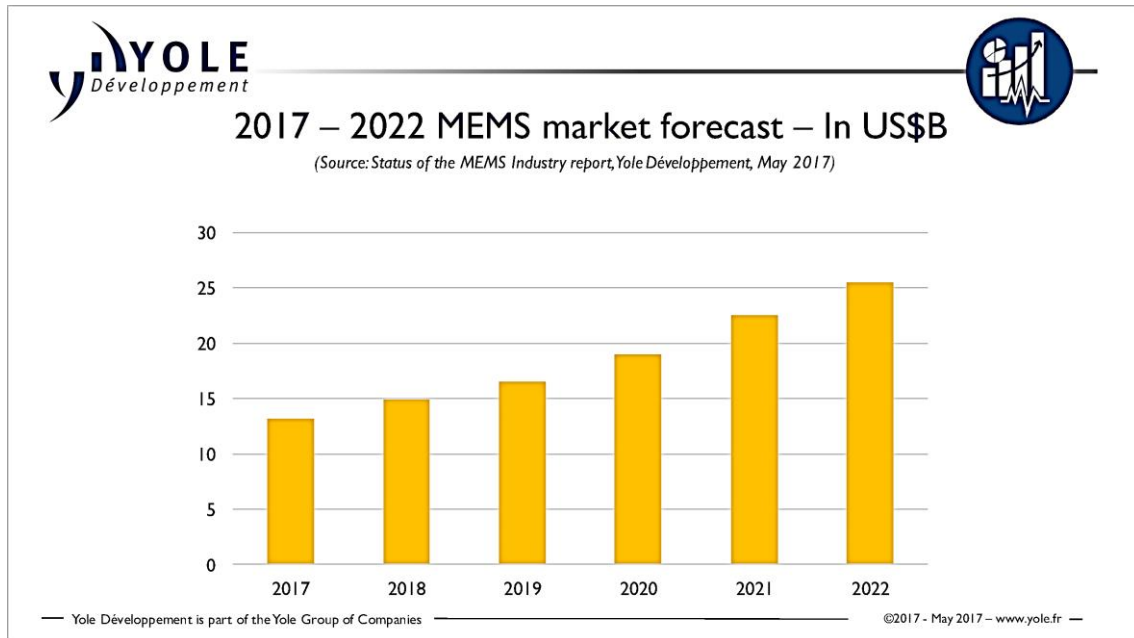


Figure 1. 2017-2022 MEMS market forecast-In US\$B (Yole Développement, May 2017) [12].

This illustrates the growing need for MEMS technology. The largest growth is expected in telecommunications systems [13]. This trend is predicted to influence the corresponding growth in RF MEMS switches [2], as RF MEMS switches are the basic components integrated into cellular base stations for switching in telecommunication networks [14]. In this research work, Aluminium nitride (AlN) piezoelectric material is employed in for the switch actuation due to its low actuation voltage, compatibility with CMOS, thermal stability, and non-toxicity [15,16].

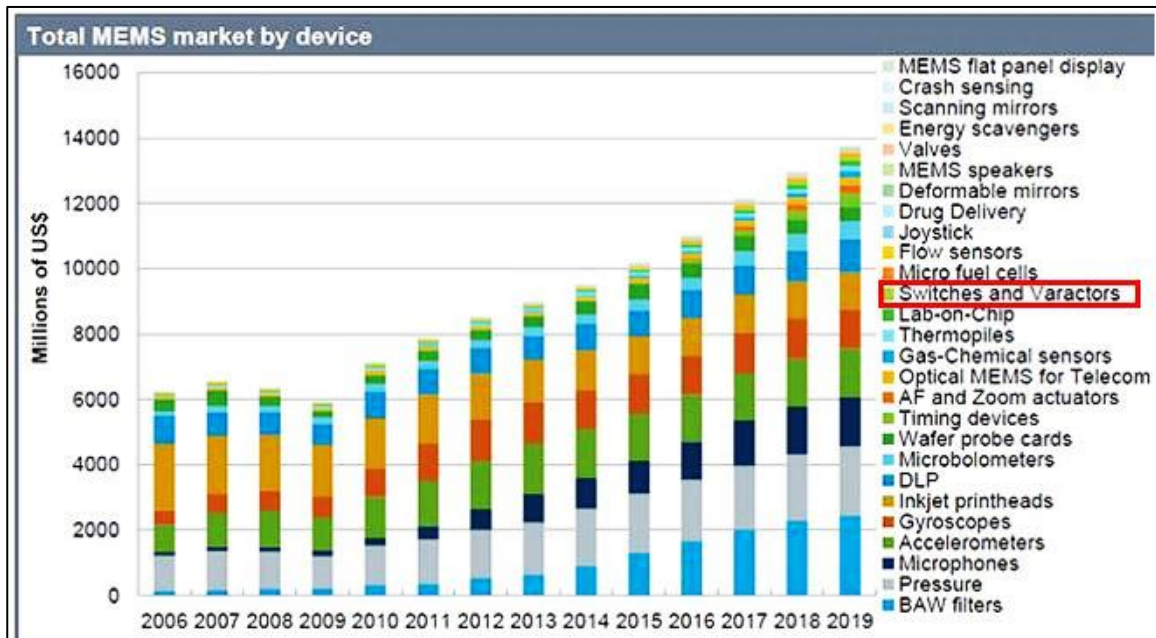


Figure 2. Total MEMS market by a. Device b. Application [13]

RF MEMS switches continue to gain momentum due to their characteristic of operating much closer to ideal switches at RF and microwave frequencies [17]. Presently, RF MEMS switches, such as Radiant and Omron RF MEMS switches controlled by electrostatic actuation, are available in the market [18]. However, a key drawback of the current electrostatically actuated RF MEMS switches is their high actuation voltage, typically in the range of 20-40 V, which makes RF MEMS switches undesirable for application in handheld wireless communication systems like mobile phones, where DC supply voltages are limited to 3-5 V [19].

## 1.5 Research objectives

In order to lower the actuation voltage, this research work investigates the piezoelectric actuation mechanism for the control of RF MEMS switches, as piezoelectric actuation has the best prospects of achieving low actuation voltage [3]. Also, because low actuation voltage can result in a compromise on the contact force [20], the main objective of this research work is to achieve low actuation voltage with adequate contact force by carrying out a parametric analysis involving some key parameters that influence these factors. The sub-objectives to be carried out in order to achieve the main objectives are as follows:

- a) Examine state-of-the-art piezoelectric-based RF MEMS switches to evaluate their performance and technological complexity.
- b) Utilise mathematical simulations/modelling to obtain optimized design parameters.

- c) Conduct a finite-element modelling (FEM) analysis for the RF MEMS switch.
- d) Validation and comparison of the mathematical modelling and finite element modelling (FEM) analyses.

The outcome of the above objectives should enable the selection of the design with the optimal ratio of the electromechanical parameters for low voltage actuation of RF MEMS switches.

## **1.6 Structure of the thesis**

This thesis is organized into six chapters. Chapter 1 provides an overview of RF MEMS technology, and the motivation and research objectives of this thesis work. Chapter 2 reports a deep analysis of state-of-the-art Piezoelectric RF MEMS switches, focusing on the optimized performance parameters and solutions proposed so far. In Chapter 3, a brief overview of the mathematical calculations underlying the design of RF MEMS switches and mathematical modelling presented. Chapter 4 offers Finite Element Modelling (FEM) for single and dual-beam cantilevers. In Chapter 5, optimization of switch designs is discussed and realised. The work will be summarized and concluded in Chapter 6, and references used, compiled.



## 2 Overview of piezoelectric materials

A piezoelectric material is a material that can generate an electric potential when mechanical stress is applied to it, using the principle of the piezoelectric effect. Conversely, these materials can also generate mechanical stress when an electric potential is applied. Three classes of materials can demonstrate the piezoelectric property; ceramics, semiconductors, and polymers. The most common piezoelectric materials explored for MEMS applications are Lead Zirconate Titanate (PZT)-ceramic, lithium niobite (LiNbO<sub>3</sub>)-ceramic, aluminium nitride (AlN)-semiconductor and Zinc oxide (ZnO)-semiconductor. Piezoelectric materials in thin form offer several advantages, such as high deflections at relatively low actuation voltages, reduced noise and power consumption, and excellent performance at high frequencies. The choice of material is application-specific and dependent on factors such as chemical composition, structure and morphology, thermal and electrical compatibility between the thin film and substrate, and their ability to withstand processing conditions without degradation [21]. An overview of the piezoelectric properties of AlN, ZnO, PZT, and LiNbO<sub>3</sub> is presented in Table 2.

Table 1. Properties of piezoelectric materials: PZT, LiNbO<sub>3</sub>, AlN and ZnO [21]

<b>Piezoelectric properties</b>	Band gap (eV)	Young modulus (GPa)	Acoustic velocity (vs)	Piezoelectric coefficient, d <sub>31</sub> (pm/V)	Relative dielectric constant, ε <sub>r</sub>	Position temperature (°C)
<b>AlN</b>	6.2	332	10127	-2	4.6	RT*
<b>ZnO</b>	3.4	20	570	-5	4.5	RT*
<b>PZT</b>	2.67	68	3900	-150	1500	500-600
<b>LiNbO<sub>3</sub></b>	4	293	3980	-7.4	29	500-700

RT \* Room temperature

PZT has been extensively explored for MEMS applications over the last two decades, because its piezoelectric constant (d<sub>31</sub>) is nearly 100 times higher than that of AlN and ZnO; hence, it has a greater tendency to provide low actuation voltages in RF MEMS switches. However, in recent times, its popularity is diminishing owing to worldwide policies discouraging the manufacture of products containing Lead, due to its toxic nature [16]. Moreover, because PZT thin film deposition occurs at temperatures over 500 °C, it is incompatible with CMOS [15], making it undesirable for future electronic devices.

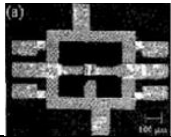
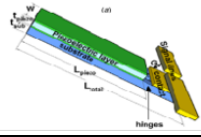
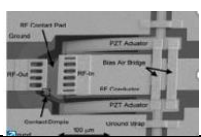
AlN and ZnO have wide bandgaps and, as such, demonstrate thermal stability at high temperatures. In addition, due to their compounds' composition, they are chemically stable and non-toxic. These properties make them desirable for applications in harsh environments [15]. Furthermore, AlN has the added advantage of CMOS compatibility. However, AlN is, by far, the least explored amongst these piezoelectric materials, due to its relatively low piezoelectric constant. This drawback of AlN can be addressed by using c-axis orientation to obtain a higher piezoelectric coefficient. The latest  $d_{31}$  value for AlN, using c-axis orientation is  $-2.7813$  pm/V [21]. These properties, together with progress on c-axis orientation, have resulted in a spike in interest in AlN as a material for low-actuation-voltage deflection devices.

Although AlN and ZnO share some similarities, ZnO has the propensity to increase its conductivity at low frequencies, leading to higher dielectric loss, and hence it becomes inapplicable for low-frequency-operated actuators and sensors. Nonetheless, LiNBO<sub>3</sub> and ZnO are very suited for energy-harvesting applications, due to their high electromechanical coupling [19].

## **2.1 Piezoelectric RF Mems Switches - State of the Art**

Duly, in a bid to reduce the actuation voltage of the RF MEMS switch for its viability in wireless and mobile applications, the focus of research in this field has shifted to exploring the piezoelectric actuation mechanism. A detailed outlook of the state of the art in Piezoelectric RF MEMs Switches for the past decade is summarised in Table 3.

Table 2. State of the art of piezoelectric RF MEMS switches

Performance parameters for PZT	Lee et al., 2004 [22]		Lee et al., 2005 [23]	Polcawich et al., 2007 [24]	Polcawich et al., 2007 [25]
Structure					
Actuation Voltage (V)	3.5	3.5	2.5	<10	10
Switch type	Resistive switch	Capacitive switch	DC contact switch	Ohmic series Switch	Ohmic series Switch
Contact Force (( $\mu$ N))	-	-	-	-	-
Frequency range (GHz)	5	5	2	50	50
Isolation (dB)	-62	-18	-42	>20dB @ 65GHz	30
Insertion Loss(dB)	-0.8	-0.7	-0.22	< 1dB @ 40GHz	0.5
Fabrication	RSBM*	CSMB *	SMB* and EP*	Surface micromachining	Surface micromachining

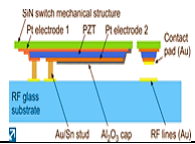
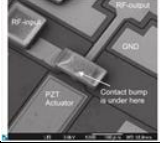
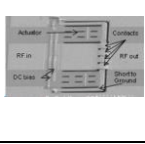
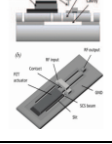
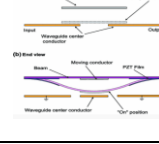
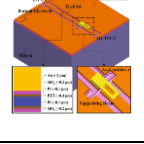
EP\* Electroplating technique

CSMB\* Capacitive-Silicon bulk

SMB\* Silicon bulk micromachining

RSBM \* Resistive-Silicon bulk micromachining

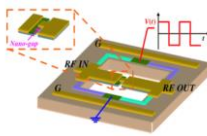
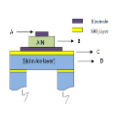
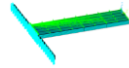
Table 3. contd. State of the art of piezoelectric RF MEMS switches

Performance parameters for PZT	Guerre et al., 2010 [26]	Nakatani et al., 2011 [27]	Ivanov et al., 2012 [28]	Katsuki et al., 2013 [29]	Giffney et al., 2015 [30]	Yu et al., 2015 [31]
Structure						
Actuation Voltage (V)	15	<15	16	20	22.4	2
Switch type	SPDT switch	Ohmic contact	Shunt	Ohmic contact	Capacitive Series	capacitive
Contact Force (( $\mu$ N))	-	-	-	-	-	-
Frequency range (GHz)	0.4-6	5	2	5	6-14	5
Isolation (dB)	30	-25	-29	-20	>10	20
Insertion Loss(dB)	0.5	-0.3	-0.6	-0.5	<0.7	0.4
Fabrication	WLFT	SCS	SOI	WLFT	SOI	TLiPMC-based

WLFT\* Wafer level transfer technologies      SCS\* single crystal silicon

SOI\* Silicon on insulator technology

Table 3. contd. State of the art of piezoelectric RF MEMS switches

Performance parameters for AlN	G. Piazza et al., 2008 [32]	N. Sinha et al., 2009 [33]	P.C. Tembhare, 2017 [34]	M.H. Ziko et al., 2018 [35]
Structure				
Actuation Voltage (V)	5-20V	27.5	40	2

Switch type	Dual-beam Switch	Capacitive		
Contact Force ( $\mu\text{N}$ )	-	-	-	100
Frequency range (GHz)	2	500MHz	2.4	
Isolation (dB)	> 26 dB	> -50 dB	31 dB	
Insertion Loss(dB)	0.67 dB	- 0.7 dB	7.8	
Fabrication	7 mask technique	contour-mode technology		

According to the state-of-the-art review, the Piezoelectric actuation mechanism can provide low actuation voltage, high isolation, low losses and low power consumption. Considering the review of piezoelectric materials, the remainder of this work will focus on AlN piezoelectric material. In addition, the substrate material that is used in RF MEMS switches also plays a role in achieving a low actuation voltage. Popular substrate materials employed in MEMS switches include silicon and Silicon nitride. However, some polymers, such as SU8, are also becoming popular, due to their lower Young's modulus value, which results in greater switch deflection. For this research work, silicon is selected as the substrate material, due to its low Young modulus value (160GPa) relative to silicon nitride (315GPa), and its popularity in mass mobile applications [35].

### 3 Modelling of RF MEMS switch

The analytical approach to the development of RF MEMS switches follows the following steps, shown in flowchart Figure 3. All the mentioned steps will be explained and analysed in detail in the upcoming sections.

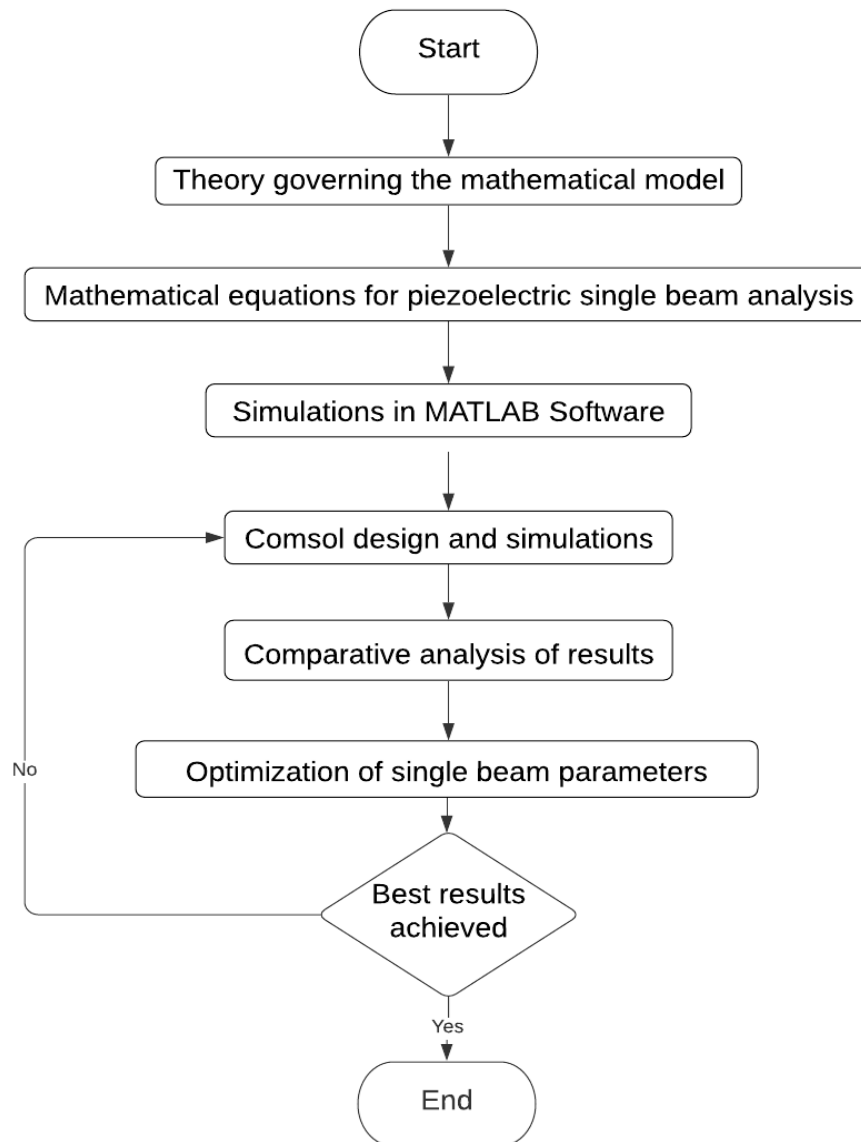


Figure 3. Flowchart for modelling RF MEMS Switch

### 3.1 Theory governing the mathematical model

The mathematical models of the single-beam RF MEMS switch are governed by the Euler-Bernoulli beam theory. The Bernoulli-Euler beam theory relies on two major assumptions [36]; that plain sections remain plane and that deformed beam slopes are small. The first assumption is illustrated in Figure 4.

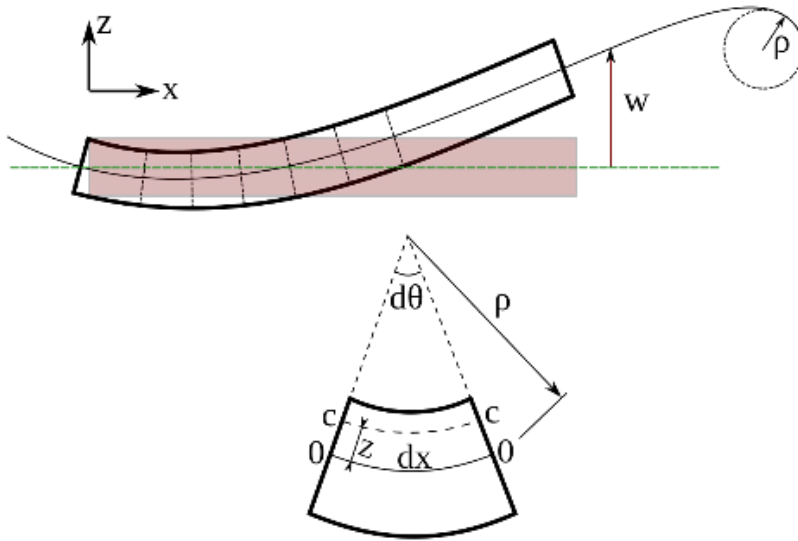


Figure 4. Euler-Bernoulli Beam Theory Assumptions: The plane section remains normal to the axis of the beam after deformation [37]

It states that any section of a beam that was a flat plane prior to the beam deforming, will remain a flat plane after the beam deflects; that is, it will not curve out-of-plane. This assumption is generally relatively valid for bending beams unless the beam experiences large shear or torsional stresses relative to the bending stresses. However, shear stresses in beams may become larger than the bending stresses when the beam is deep and short in length. In order to conform to these assumptions, the beam length to be modelled is relatively long, with small deflections expected.

### 3.2 Structure of the piezoelectric cantilever beam model

The proposed RF MEMS switch shown in Figure 5 is a single beam cantilever, made up of a piezoelectric layer and a substrate layer of the same length and width. In this model, the piezoelectric layer consists of AlN material, and the substrate layer is made of silicon.

For analytic purposes, the piezoelectric layer is assumed to be perfectly placed on the substrate layer. The length of the beam is denoted  $L$ , and the switch gap is denoted  $G$ , the thickness of the substrate and piezoelectric layers are denoted as  $t_b$  and  $t_p$  respectively.

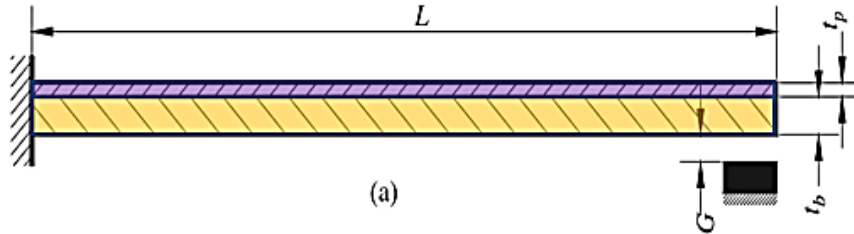


Figure 5. Piezoelectric cantilever beam model [38]

### 3.3 Mathematical modelling of displacement

When DC voltage is applied to the piezoelectric layer, the beam deflects either upward or downwards in response to the applied voltage, as shown in figure 6. The X-axis runs from the fixed end to the free end of the cantilever, and corresponds to a value of zero at the fixed end, whereas the Y-axis lies at the thickness of the beam and corresponds to a value of zero at the interface between the layers (AlN and Si). The displacement of the beam is derived following the mathematical steps below, using the principles of the Euler-Bernoulli beam theory, since the modelled beam is long, and as such its shear deformation is negligible [3,38].

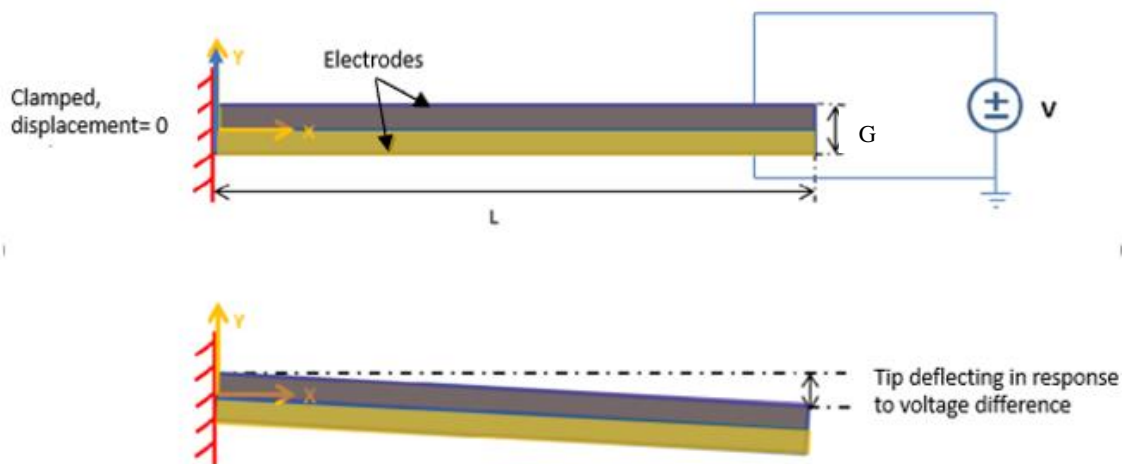


Figure 6. Deflection of piezoelectric switch in response to applied voltage [39]



The cross-sectional areas of the substrate ( $A_b$ ) and the piezoelectric layer ( $A_p$ ) are given as

$$A_b = W \cdot t_b \quad (1)$$

$$A_p = W \cdot t_p \quad (2)$$

And the moments of inertia for the substrate ( $I_b$ ) and the piezoelectric layer ( $I_p$ ) are given as

$$I_b = (W \cdot t_b^3)/12 \quad (3)$$

$$I_p = (W \cdot t_p^3)/12 \quad (4)$$

Where  $W$  is the width of the beam,  $t_b$  the thickness of substrate and  $t_p$  the thickness of the piezoelectric layer.

The free piezoelectric strain, assuming the strain distribution on the piezoelectric layer is dominated by the deflection pattern of the substrate, is given as

$$\xi_0 = (V \cdot d_{31})/t_p \quad (5)$$

where  $V$  is the actuation voltage,  $d_{31}$  is the piezoelectric coefficient of the actuator layer and  $t_p$  is the thickness of the piezoelectric layer.

For piezoelectric cantilevers, shear and normal stresses at all interfaces except the film edge are zero, and with constant internal cross section. Hence, piezoelectric actuation is only represented by a line-distributed shear force and bending moment applied at the film edges.

The distributed shear force is defined by the equation

$$T = \xi_0 \left( \left( \left( \frac{1}{E_p A_p} \right) + \left( \frac{1}{E_b A_b} \right) \right) + \left( \left( \frac{t_b^2}{4E_b A_b} \right) + \left( \frac{t_p^2}{4E_p A_p} \right) \right) + \left( \left( \frac{t_p t_b}{4E_p A_p} \right) - \left( \frac{t_b^2}{4E_b A_b} \right) \right) \cdot \left( \frac{(r t_b - t_p)}{(1+r)t_b} \right) \right) \quad (6)$$

Where  $r$  is given as

$$r = \left( \frac{E_p I_p}{E_b I_b} \right) \quad (7)$$

$E_p$  and  $E_b$  are the Young's modulus of the piezoelectric layer and the substrate, respectively.

The piezoelectric bending moment of the AlN unimorph cantilever RF MEMS switch is defined by the equation:

$$M_s = \left(\frac{1}{1+r}\right) \left(\frac{t_b+t_p}{2}\right) T \quad (8)$$

Substituting T from equation 6 into equation 8,

$$M_s = \left(\frac{1}{1+r}\right) \left(\frac{t_b+t_p}{2}\right) \frac{\xi_o}{\left(\left(\left(\frac{1}{E_p A_p}\right) + \left(\frac{1}{E_b A_b}\right)\right) + \left(\left(\frac{t_b^2}{4E_b A_b}\right) + \left(\frac{t_p^2}{4E_p A_p}\right)\right) + \left(\left(\frac{t_p t_b}{4E_p A_p}\right) - \left(\frac{t_b^2}{4E_b A_b}\right)\right) \cdot \left(\frac{(rt_b - tp)}{(1+r)t_b}\right)\right)} \quad (9)$$

Hence, the static tip displacement of the AlN unimorph cantilever is derived as

$$Disp = \left(\frac{M_s L^2}{2E_b I_b}\right) \quad (10)$$

### 3.4 MATLAB simulations

The objective of this chapter is to gain an understanding of how geometric parameters and some material properties of the single beam affect the overall performance of the RF MEMS switch. To achieve this, parametric studies are carried out to investigate the effect of the geometrical parameters on these factors. The parametric studies are implemented using MATLAB simulation software, which allows for multiple geometry parameter changes in a unique study. The thickness of the piezoelectric film,  $t_p$ ; substrate thickness,  $t_b$ ; width of the switch,  $W$ ; length of beam,  $L$ ; and the piezoelectric coefficient,  $d_{31}$ , on the tip deflection, actuation voltage and contact force will be explicated. A range of variable geometric parameters which can be applied in practice is considered for these simulations. The geometry and material properties of the single beam cantilever switch system are listed in Table 4. The results of these simulations will be used to obtain optimized switch design parameters, to achieve high beam deflection at low actuation voltage and high contact force.

Table 3. Geometry and material properties of the proposed switch model

Parameter [units]	Value
Young's modulus of piezo, $E_p$ [GPa]	308
Young's modulus of substrate, $E_b$ [GPa]	169
Piezoelectric coefficient, $d_{31}$ [pm/V]	-2.7
Beam Length, L [ $\mu\text{m}$ ]	2500
Beam Width, W [ $\mu\text{m}$ ]	500
Thickness of piezo, $t_p$ [ $\mu\text{m}$ ]	0.5
Thickness of substrate, $t_b$ [ $\mu\text{m}$ ]	50
Initial switch air gap G [nm]	500

### 3.4.1 Beam deflection analysis

Table 5 provides an overview of the six simulations which are considered and their associated parameter variations:

Table 4. Order of simulations for displacement analysis

Parameter	Simulation 1	Simulation 2	Simulation 3	Simulation 4	Simulation 5
Length	✓	✓	✓	✓	✓
Width			✓		
Piezoelectric thickness	✓				
Substrate thickness		✓			
Applied Voltage				✓	
Piezoelectric coefficient ( $d_{31}$ )					✓

### 3.4.2 Effect of piezoelectric thickness

The relationship between the beam deflection and the piezoelectric AlN thickness is demonstrated in Figure 7. A set of beam length values ranging from 1000  $\mu\text{m}$  to 2500  $\mu\text{m}$  and piezoelectric thickness ranging from 0.5  $\mu\text{m}$  to 2.5  $\mu\text{m}$  are the variables used in this simulation. All other parameters are fixed. Although the mathematical formula relating the tip displacement and the piezoelectric thickness is not straightforward, the simulation using the MATLAB tool depicts this relationship in a clear manner.

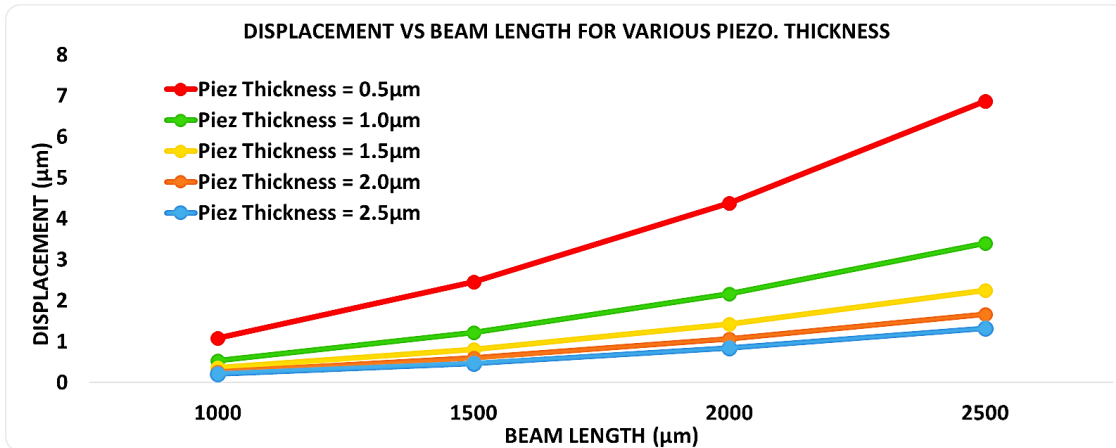


Figure 7. Displacements versus beam length for varying piezoelectric thickness

Figure 7 compares the tip displacement of the single-beam RF MEMS switch for the different piezoelectric thickness. Overall, it can be observed that the tip displacement declines as the piezoelectric thickness increases. Hence, at the minimum  $t_p$  value of  $0.5 \mu\text{m}$ , the highest displacement value of  $6.8 \mu\text{m}$  was obtained at beam length of  $2500 \mu\text{m}$ . However, a sharp decline in the displacement of about 50% is observed as  $t_p$  increases from  $0.5 \mu\text{m}$  to  $1 \mu\text{m}$ . The overall decline in displacement in response to the increase in piezoelectric thickness could be attributed to the decline in strain on the top surface as the thickness of the piezoelectric layer increases. The decrease in strain causes the beam stiffness to increase, which results in a reduced deflection. Although the change in deflection in response to piezoelectric thickness is not dramatic, it is recommended that, in obtaining an optimized switch geometry, the  $t_p$  value should be as small as possible.

### 3.4.3 Effect of substrate thickness

Secondly, the influence of substrate thickness  $t_b$  on beam displacement is examined. This parametric study utilizes a set of beam length values and a range of values from  $50 \mu\text{m}$  to  $100 \mu\text{m}$  as substrate thickness, while all other parameters remain fixed. Mechanically, it is expected that, as the substrate thickness increases, the position of the neutral axis will shift away from the piezoelectric layer and move into the substrate layer. Consequently, the axial stress along the beam will increase, causing the beam stiffness to reduce. The beam deflection is expected to decrease as a result of this. Figure 8, obtained from the MATLAB simulation, demonstrates beam displacement behaviour in response to changes in substrate thickness.

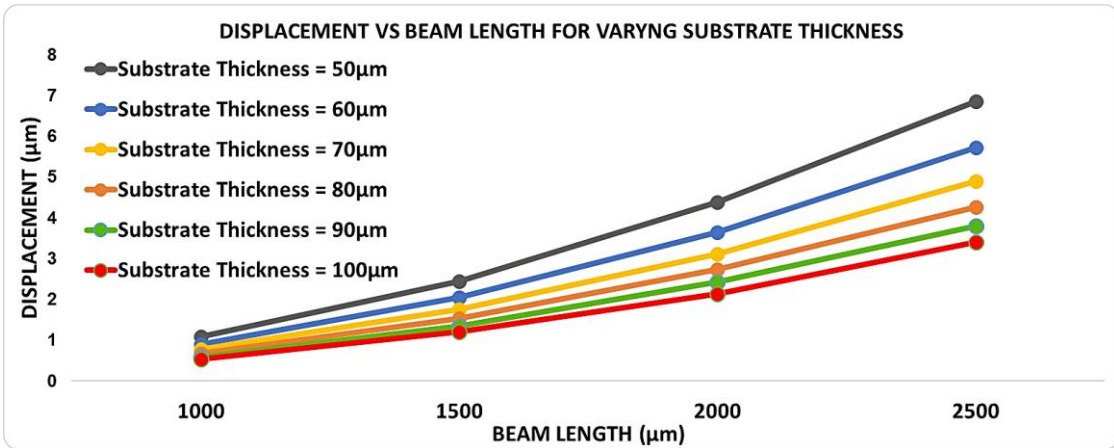


Figure 8. Displacement versus beam length for varying substrate thickness

The displacement is observed to continuously decrease as the substrate thickness increases. Hence, the lowest  $t_b$  value of 50 μm produces the highest deflection of 6.8 μm at beam length of 2500 μm. It is recommended that the substrate thickness should be kept as small as possible in the optimized beam geometry. However, the substrate thickness should not be so small as to make the beam fragile and difficult to handle.

### 3.4.4 Effect of beam width

Next, the effect of beam width is briefly examined using the simulation result presented in Figure 9. In this switch model, the substrate has the same width as the piezoelectric layer. The simulation utilizes a set of beam length values and four different values for beam width, while keeping all other parameters unchanged. The beam width range used for this simulation is 100 μm to 500 μm.

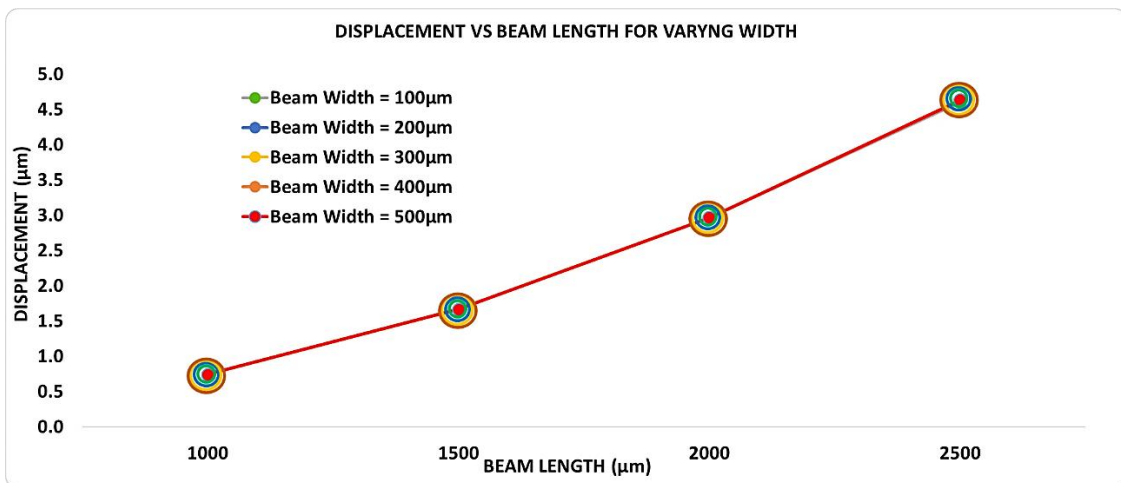


Figure 9. Displacement versus beam length for varying beam width

Figure 9 shows that the displacement trend remains unchanged as we vary the beam width. This result indicates that, in the case when the width of the top layer is the same as the bottom layer, then change in width produces the same displacement trend regardless of the beam length.

### 3.4.5 Effect of actuation voltage

Figure 10 shows the outcome of simulation 4, illustrating the voltage response of the piezoelectric cantilever switch. This simulation uses a set of beam length values and low actuation voltage values of the range 1V to 9V, while all other parameters remain fixed.

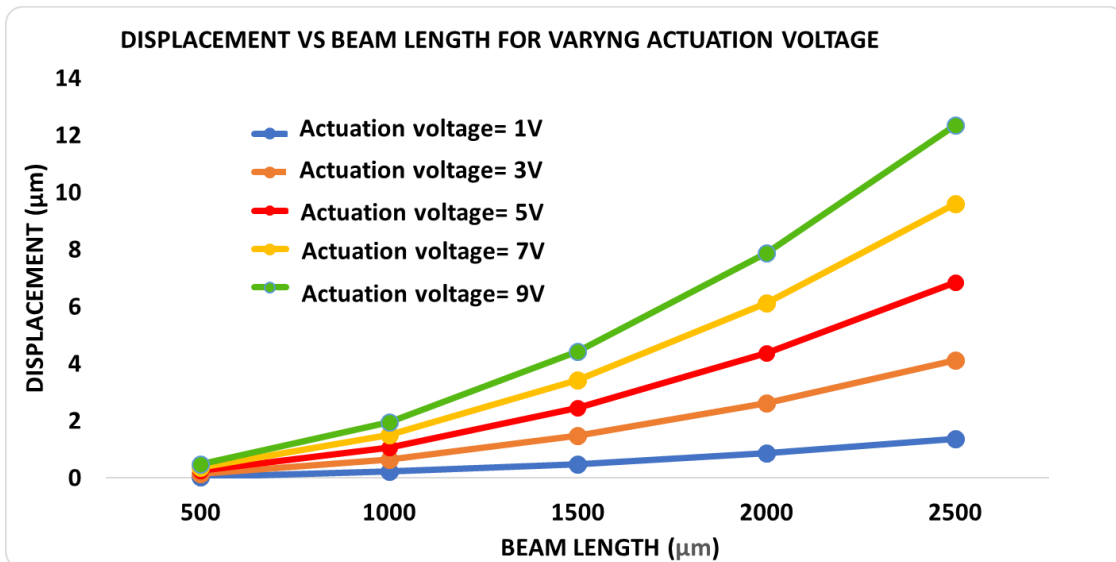


Figure 10. Displacement versus beam length for varying actuation voltage

From the graph, it is seen that displacement is an increasing function of actuation voltage. In the next session, factors that affect actuation voltage of the switch are discussed and some simulations conducted are evaluated.

### 3.5 Mathematical modelling of actuation voltage

Recalling that one major research goal is to obtain low actuation voltage for the operation of RF-MEM switches, the mathematical equation relating applied voltage to switch geometry and material properties is shown as equation 11.

$$V = \frac{2E_b I_b G}{k d_{31} L^2} \quad (11)$$

Where  $k$  is the proportionality factor and is calculated;

$$k = \frac{\frac{t_b}{2t_p}}{\frac{1}{E_b A_b} + \frac{t_b(t_b+t_p)}{4E_b I_b} + \frac{1}{E_p A_p}} \quad (12)$$

These two straightforward equations imply that, in order to obtain a required and optimum deflection at low voltage, three methods can be explored. The first method is to use a small initial gap size between the switch and the suspended RF signal line. According to equation 11, if the air gap is reduced, then the actuation voltage required by the RF MEMS switch also decreases. However, the reduced air gap will result in a compromise on the isolation and lead to high insertion losses, due to the up-state capacitance introduced, especially for the capacitive-type RF MEMS switch. These limitations can, however, be mitigated by adding T-type and Pi-matching circuits to counter the effects of parasitic capacitance, or by designing the switch with a comb structure which is actuated laterally [39].

The second method is by increasing the effective area of the piezoelectric actuator. The effective cross-sectional area can be increased by increasing the length or width or both. By increasing the cross-sectional area of the switch, the proportionality factor  $k$  is reduced, which in turn reduces the actuation voltage. However, in implementing this method, it is necessary to impose limits to the miniaturization as much as possible. The third method of reducing the voltage is by reducing the spring constant of the cantilever by using folded beams, serpentine beams and hollow triangular beams. The third methods can also be achieved by increasing the width of the beam. Figure 11 shows the simulation result for displacement vs actuation voltage for varying length.

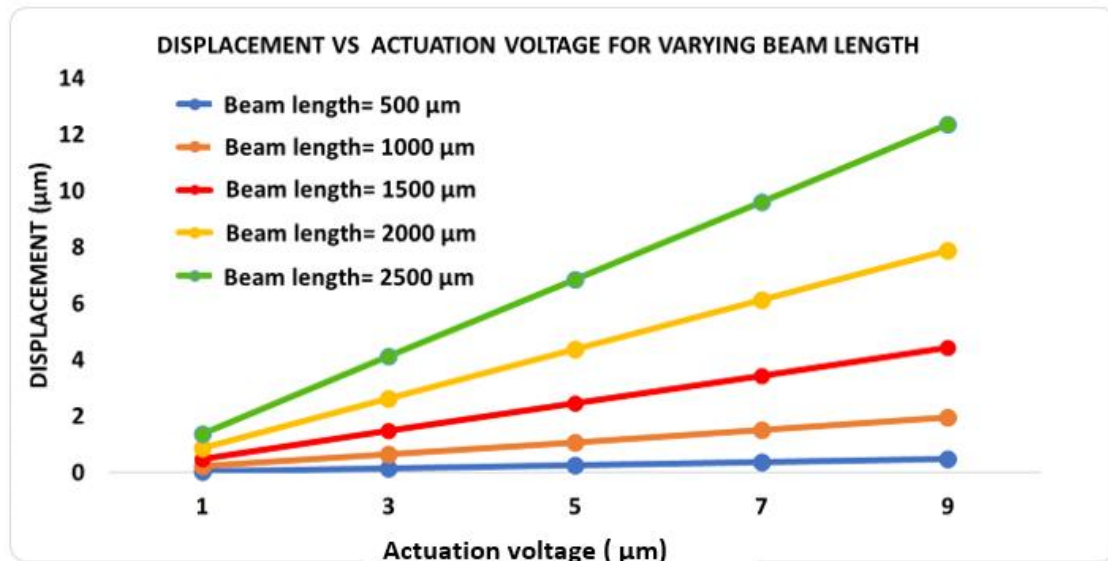


Figure 11. Displacements vs actuation voltage for varying beam length

It can be observed from the result above that, as the beam length increases, the required actuation voltage to attain any displacement reduces considerably. Furthermore, the material properties of the beam also play a significant role in achieving large displacements at low voltages. For instance, the simulation plot of displacement vs actuation voltage for varying piezoelectric coefficient  $d_{31}$ , illustrated in Figure 11., shows that, the higher the  $d_{31}$  value, the lower the voltage required to achieve required displacement. It has been found in research that the  $d_{31}$  value of AlN material can be increased using c-axis orientation in the fabrication of the piezoelectric film [3].

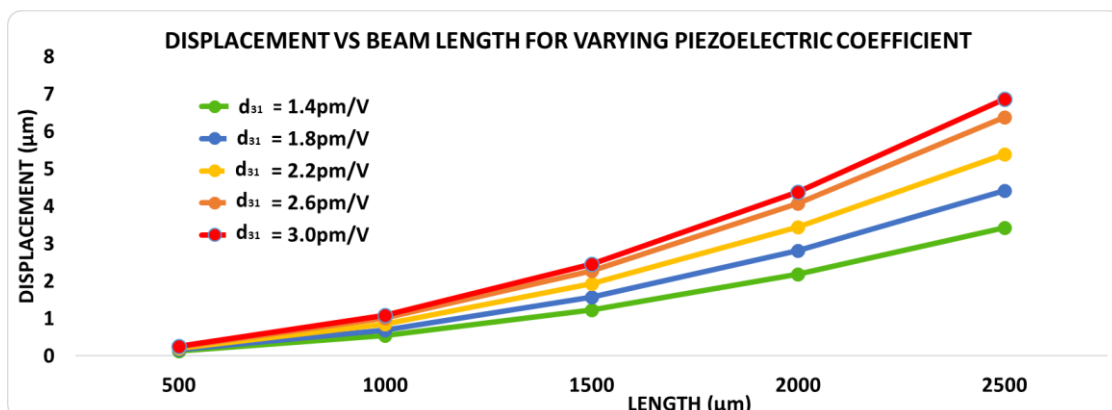


Figure 12 Displacements versus beam length for varying piezoelectric coefficient



### 3.6 Mathematical modelling of contact force

Ensuring adequate contact force at the contact region of the switch is important for the overall performance of the switch. This is because, at the appropriate contact force, adhesion at the surface of the contacts is sufficiently large to prevent the opening of the contact at the on-state. On the other hand, when the contact force is insufficient, only a few sections of the contact surface remain in contact. If this separation at the contact continues, then little or no RF signal will be transmitted through the interface [40]. Figure 13 illustrates the beam deflecting and establishing contact at the contact surfaces, by closing the initial switch gap,  $G$ .



Figure 13. Contact force acting at switch contact region [41]

Contact force is dependent on the initial switch gap, contact geometry and switch geometry. The mathematical equations below represent the relationship between these factors.

The contact force equation is derived as

$$F_C = \left( \frac{M_e}{2(EI)_e} L^2 - G \right) \frac{3(EI)_e}{L^3} \quad (13)$$

Where  $M_e$  is the equivalent actuation bending moment due to the dynamic behaviour of the single beam,  $G$  denotes the initial switch Gap,  $L$  denotes the length of the beam, and  $(EI)_e$  denotes the equivalent flexural rigidity.

The equivalent bending moment is derived in terms of the piezoelectric bending moment  $M_s$  as

$$M_e = \frac{(EI)_e M_s}{E_b I_b} \quad (14)$$

Where the equivalent flexural rigidity  $(EI)_e$  is given as

$$(EI)_e = \frac{Wt_b^3 t_p E_b E_p}{12(E_p t_b + E_p t_p)} \cdot \left( 4 + 6 \frac{t_p}{t_b} + 4 \left( \frac{t_p}{t_b} \right)^2 + \frac{E_p}{E_b} \left( \frac{t_p}{t_b} \right)^3 + \left( \frac{E_b t_b}{E_p t_p} \right) \right) \quad (15)$$

### 3.7 MATLAB simulations

Using mathematical equation 13, derived from equations 14 and 15, the optimum geometry parameters relating to contact force are simulated in MATLAB software. In six simulations, the effect of the switch gap, beam length actuation voltage, and material property (piezoelectric coefficient) are examined in the order listed in Table 6.

Table 5. Order of simulations for contact force analysis

Parameter	Simulation 1	Simulation 2	Simulation 3	Simulation 4
Length		✓		
Width			✓	
Piezoelectric thickness				
Substrate thickness	✓	✓	✓	
Applied Voltage				✓
Switch Gap	✓			

#### 3.7.1 Effect of switch gap

Figure 14 illustrates the effect of the switch gap on the contact force. This simulation uses a set of substrate thickness values in the range of 50µm to 100µm and four different values for the initial switch gap (500nm, 1µm, 2µm, 3µm, 4µm), while all other parameters remain the same as in Table 4.

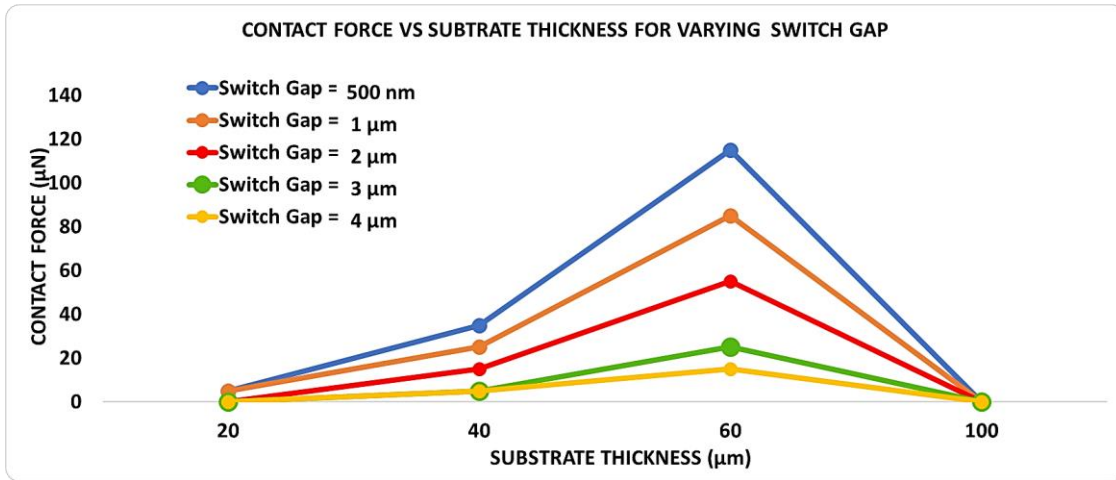


Figure 14. Contact force versus beam length for varying switch gap

From the graph, it is seen that the contact force is a decreasing function of the initial gap. The graph also illustrates that at a certain beam thickness the contact force begins to be reduced. The switch gap also affects the electrical properties of the switch, such as insertion losses. For instance, reducing the switch gap, caused the insertion losses to increase.

### 3.7.2 Effect of beam length and width

Next, the effect of beam length on contact force is analysed in Figure 15. The width and thickness of the microcantilever piezoelectric layer are fixed at 500 µm and 0.5 µm, respectively, while the length of the beam is varied from 500-2500 µm over a variable substrate thickness. Next, the effect of the beam width on displacement is observed in Figure 16. The length and thickness of the microcantilever piezoelectric layer are fixed at 2500 µm and 0.5 µm, respectively, while the width is varied over a substrate thickness range of 50-100 µm.

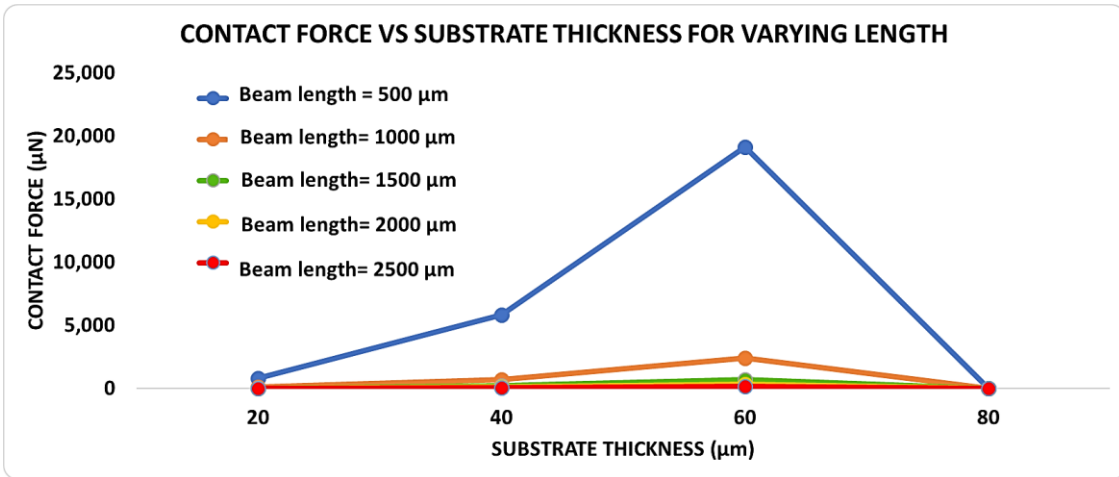


Figure 15. Contact force versus substrate thickness for varying length.

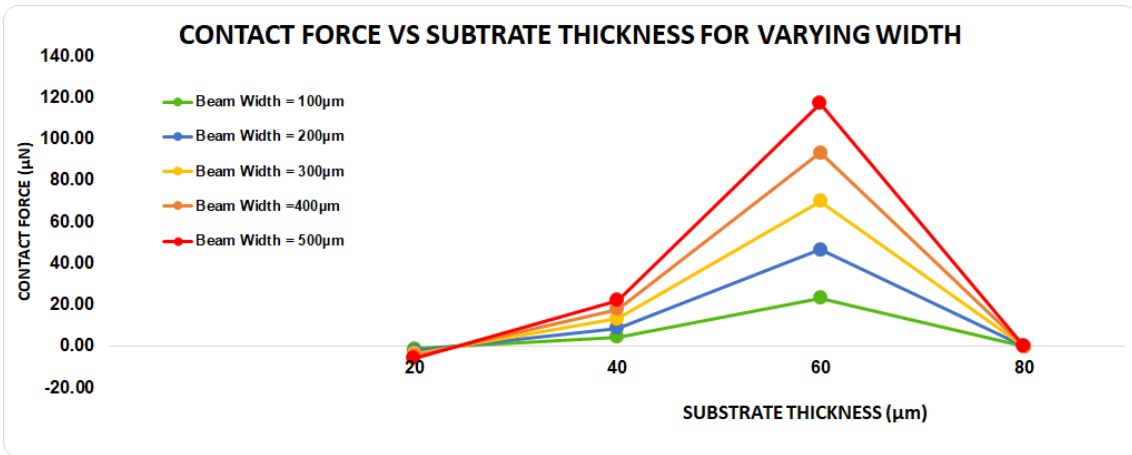


Figure 16 Contact force versus substrate thickness for varying beam width

From Figure 15, it is observed that the contact force is inversely proportional to the length of the cantilever. As well, from Figure 15, a dramatic decrease in contact force is observed as the length is increased from 500 µm to 1000 µm. The decline in contact force as the length increases can be attributed to the reduction in stiffness, since stiffness is inversely proportional to the cube of length, and directly proportional to the contact force. Contrary to the effect of the beam length, the contact force continuously increases as the beam width is increased, as depicted in Figure 16. A plausible explanation for this behaviour is that the increase in width increases the moment of inertia of the beam. Consequently, the stiffness of the beam is increased, resulting in the increase in contact force. As previously mentioned, increasing the width of the beam increases its cross-sectional area. Hence, this method of achieving high contact force should be implemented in such a way as not to exceed the limits imposed by miniaturization.

### 3.7.3 Effect of piezoelectric thickness

Next, the effect of piezoelectric thickness on contact force is examined using Figure 17. The width and thickness of the length of microcantilever are fixed at 500  $\mu\text{m}$  and 2500  $\mu\text{m}$ , respectively, while the piezoelectric thickness is varied from 0.5  $\mu\text{m}$  to 5  $\mu\text{m}$  over a variable substrate thickness.

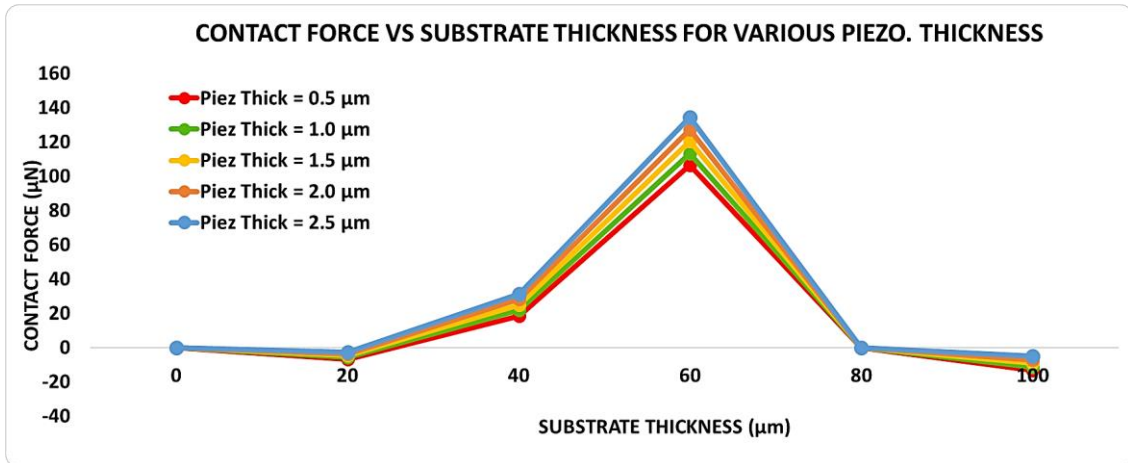


Figure 17. Contact force versus substrate thickness for varying piezoelectric thickness

It is observed from Figure 17 that the contact force decreases slightly as the piezoelectric thickness is increased.

### 3.7.4 Effect of actuation voltage

The aim of this work is to achieve a low actuation voltage and high contact force. The relationship between these two factors is simulated and examined. Contact force as a function of low actuation voltages in the range of 1-9V is shown in Figure 18.

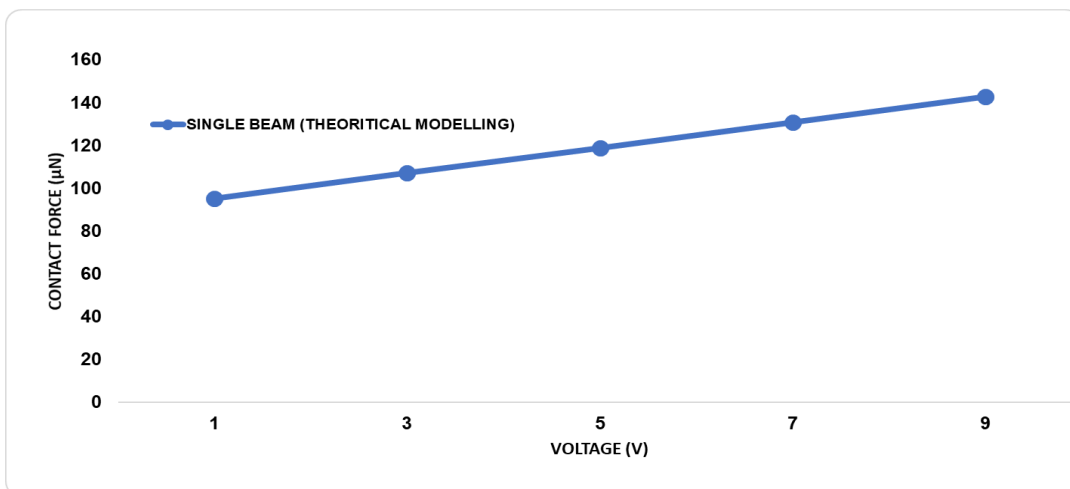


Figure 18. Contact force versus actuation voltage

Clearly, the graph illustrates that contact force increases linearly as the actuation voltage increases. As the purpose of the work is to obtain low actuation voltage and adequate high contact force, there is a need to optimize the beam geometrical parameters. Hence optimization analysis for both actuation voltage and contact force will be carried out in later sessions.

## 4 Finite element modelling of RF MEM switches

The use of the finite element software in solid modelling facilitates the implementation of material properties that are obtained from the analytical simulations. Results obtained from FEM simulation for parametric analysis are compared to mathematical simulation results. The flowchart in Figure 19 briefly describes the steps involved in carrying out the parametric analysis using the COMSOL Multiphysics tool. These steps will be explained in the following sections. These steps will be explained in the following sections.

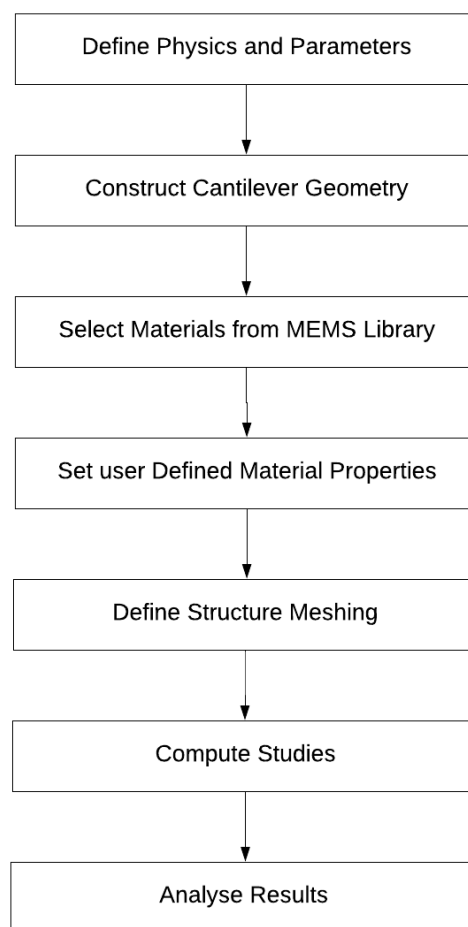


Figure 19. Modelling process steps for RF MEMS switch in COMSOL

### 4.1 RF MEMS switch structures used in COMSOL

In addition to the cross-sectional dimensions of the microcantilever, the geometrical structure (shape and make-up) plays an important role in the RF performance of the switch. FEM analysis is simulated involving four different cantilever designs. A

comparison of results obtained from simulations using these various designs will be analysed and discussed.

The first structure, as shown in Figure 20(a), is a single beam consisting of 3 layers, viz. poly-silicon as substrate layer, Silicon dioxide ( $\text{SiO}_2$ ) as insulation/buffer material, Aluminium Nitride (AlN) as the piezoelectric material. Silicon dioxide ( $\text{SiO}_2$ ) blocks the DC control signal from shorting out during switch activation. One end of the structure is clamped to provide support for the beam and increase its bending. The second structure, as shown in figure 20(b), is a double beam consisting of two single beams facing each other and meant to deflect in opposite directions. The third structure is similar to the second structure; the only difference is that the third structure has gold (Au) metal contact on top of one of the beams, as shown in figure 20(c). Gold was chosen as the contact material because of its low contact resistance, low force and its excellent surface inertness [41]. The fourth structure, as shown in Figure 20(d), is built on the third structure, with the only difference being that the fourth structure has holes (twelve holes each of  $0.2 \mu\text{m}$  diameter) perforated on the gold contact edge. Generally, creating holes in beams reduces the stiffness on deflection [42]. Double beam designs have been included in the FEM analysis, because research carried on the double beam recently indicates that a double beam shows lower resistance for a given voltage compared to a single beam. The lower contact resistance in double beam results in the increase in force per unit applied voltage [32]. Therefore, these structural differences have an impact on the required actuation voltage and contact force for optimum performance.



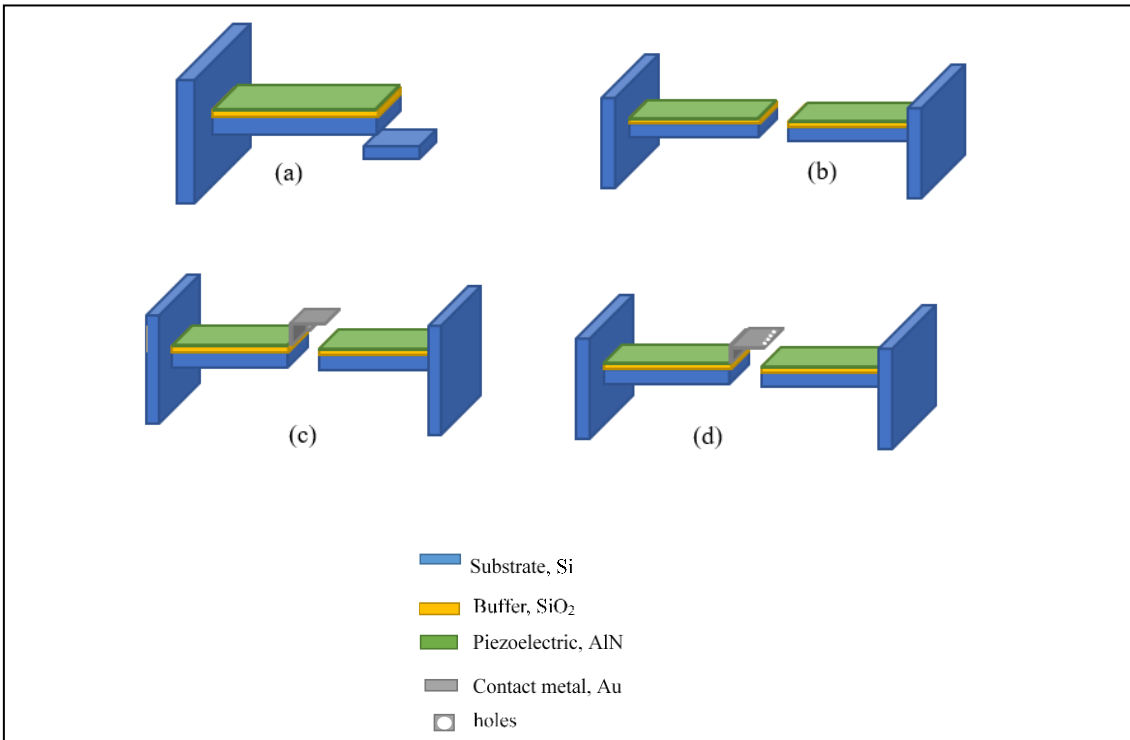


Figure 20. Proposed cantilever designs used in FEM analysis

## 4.2 Material properties

The properties of these materials relevant to COMSOL simulations, as well as the initial geometry dimensions, are listed in Table 7. The material properties considered for AlN COMSOL models are anisotropic.

Table 6. Material properties and dimensions

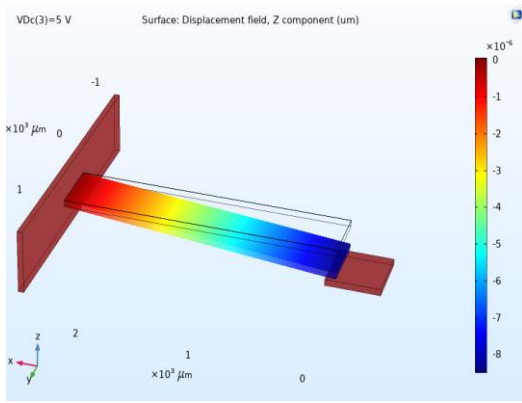
Parameter [units]	AlN	Si	SiO <sub>2</sub>	Au
Young's modulus [GPa]	308	169	70	79
Poisson ratio, $\nu$	0.22	0.3	0.17	0.44
Piezoelectric coefficient, $d_{31}$ [pm/V]	-2.7	-		-
Density, $\rho$ [kg/m <sup>3</sup> ]	3260	2330	2200	19300
Beam Length, L [ $\mu\text{m}$ ]	2500	2500	2500	0.7
Beam Width, W [ $\mu\text{m}$ ]	500	500	500	500
Thickness of layer, t [ $\mu\text{m}$ ]	0.5	50	1	0.5

### 4.3 Simulation setup

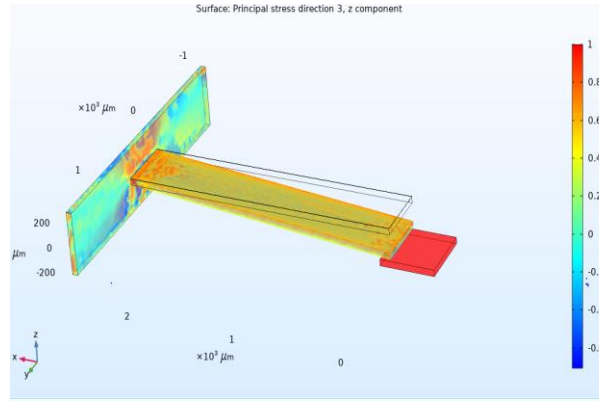
Simulations were performed on each of the four cantilever designs. The COMSOL models used are a structural mechanics module and a piezoelectric devices module. The structural model is used to simulate the mechanical behaviour, while the piezoelectric devices module is used to simulate the piezoelectric properties of the AlN layer. To carry out these parametric studies, first, the cross-sectional dimensions of the geometry under consideration are defined. Next, the materials are defined, and the user-defined parameters of these materials are entered. One end of the cantilever is assigned a fixed boundary constraint, while the other end is given a free boundary condition. For the single beam, a constant DC voltage is applied by keeping the bottom of the beam as ground and setting the top surface of the piezoelectric layer at a floating potential condition. For the three double beam designs, voltages of opposite polarity are applied to the beams. Because we want to operate the switch in a low voltage regime, an actuation voltage of 5V is applied in all four different cantilever designs.

### 4.4 3D Model results obtained

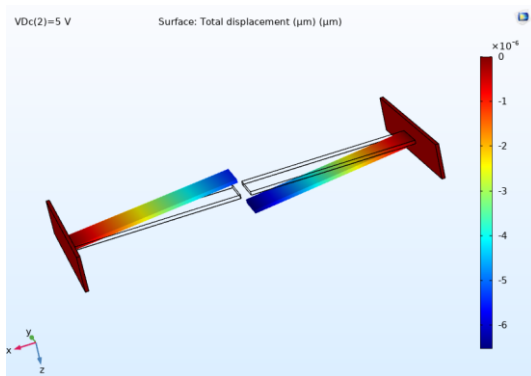
A 3D model of the simulation results obtained is shown in Figure 21. Figure 21 (a-h) depicts the results related to the displacement and stress generated and for the various geometries simulated at a constant voltage of 5 V. Parametric analysis will determine the best suited geometrical design and dimensions of the cantilever-type switch for low voltage and high contact force. Fig. 21(a-d). illustrates the 3D z-direction displacement distribution, while Fig. 21(e-h) demonstrate the von Mises stress distribution of the membrane and beams, when the actuation voltage of 5V is applied. The Mises stress distribution is used to check whether the design is sustainable at given constraints and loading conditions [42]. The stress distribution values recorded for all switch structures are  $0.01\text{MN/m}^2$ .



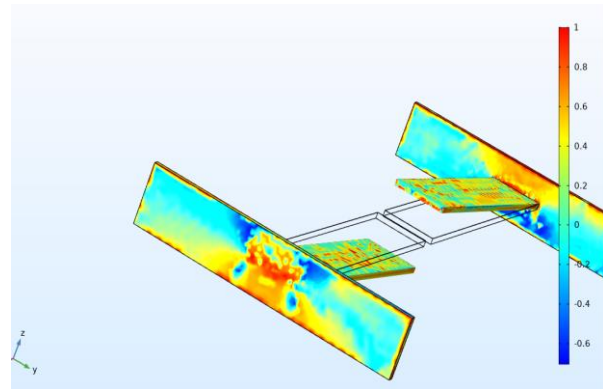
21(a). Displacement field of Single beam



21(b). Stress for single beam

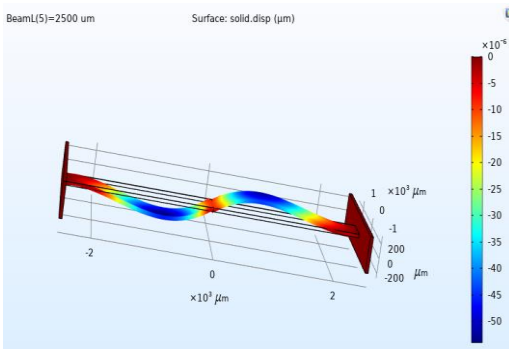


21(c) Displacement of dual beam

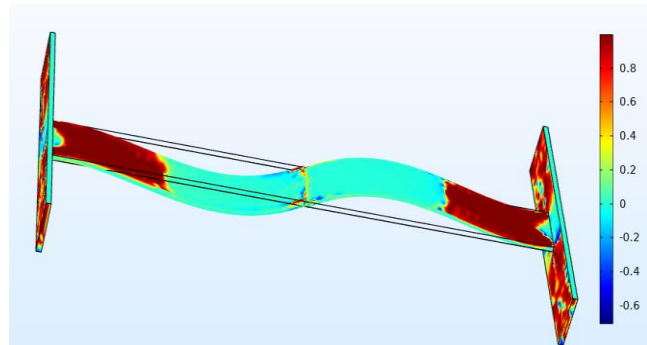


21(d) Stress for dual beam

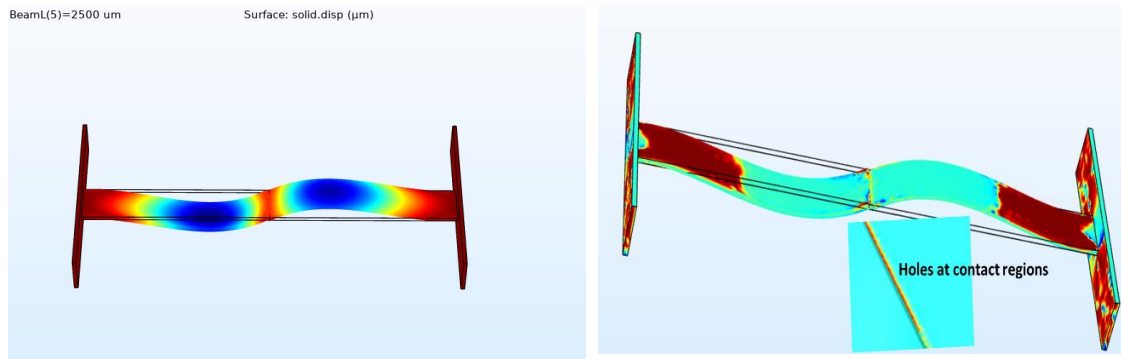
63



21(e) Displacement dual beam (Au contact)



21(f) Stress dual beam (Au contact)



21(g) Displacement dual beam (Au contact with holes)      21(h) Stress dual beam (Au contact with holes)

Figure 21. 3D model for displacement field and stress distribution.

## 4.5 Deflection analysis

The results of the various parametric studies carried out are analysed and discussed. First, a comparison is made between mathematical modelling results from MATLAB and FEM simulation for a single beam. It is important to mention that, in the switch mathematical model, the thin SiO<sub>2</sub> buffer layer and cantilever anchor are not included. However, the absence of these is not expected to cause significant variations in results relative to COMSOL results.

### 4.5.1 Comparative analysis for varying beam length

The effect of beam length on displacement for the various geometries is analysed in this section. For the COMSOL simulation, the beam width of 500  $\mu\text{m}$ , substrate thickness of 50  $\mu\text{m}$ , the piezoelectric thickness of 0.5  $\mu\text{m}$ , and constant applied voltage of 5 V are maintained. The beam length is varied from 500  $\mu\text{m}$  to 2500  $\mu\text{m}$ , at an interval of 500  $\mu\text{m}$ . Results obtained are used for the comparative studies illustrated in Figures 22 and 23.

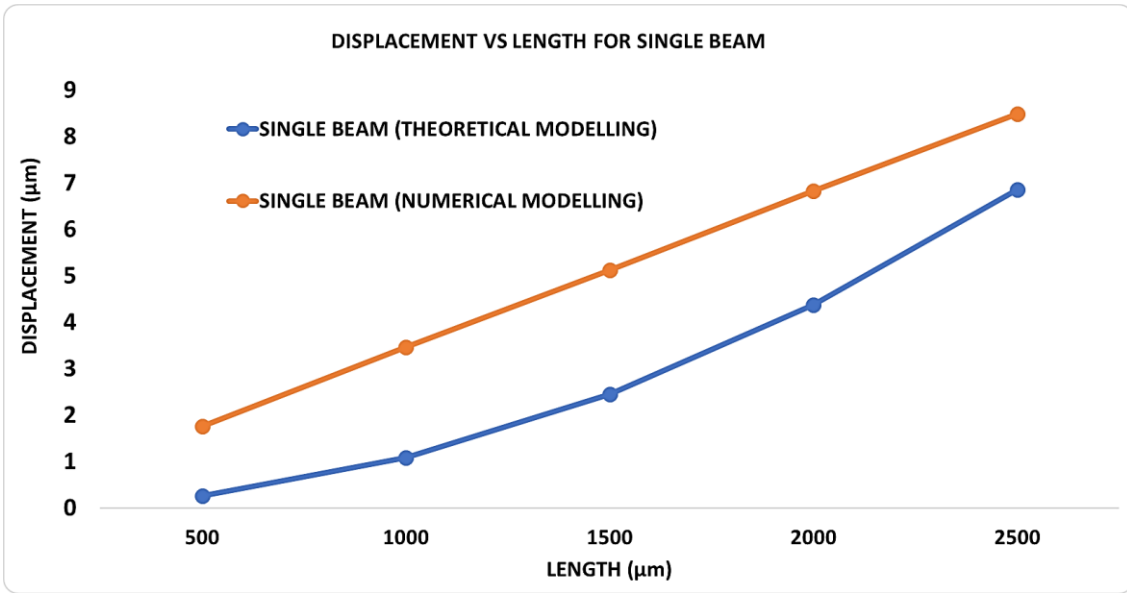


Figure 22. Displacement versus beam length plot for single beam

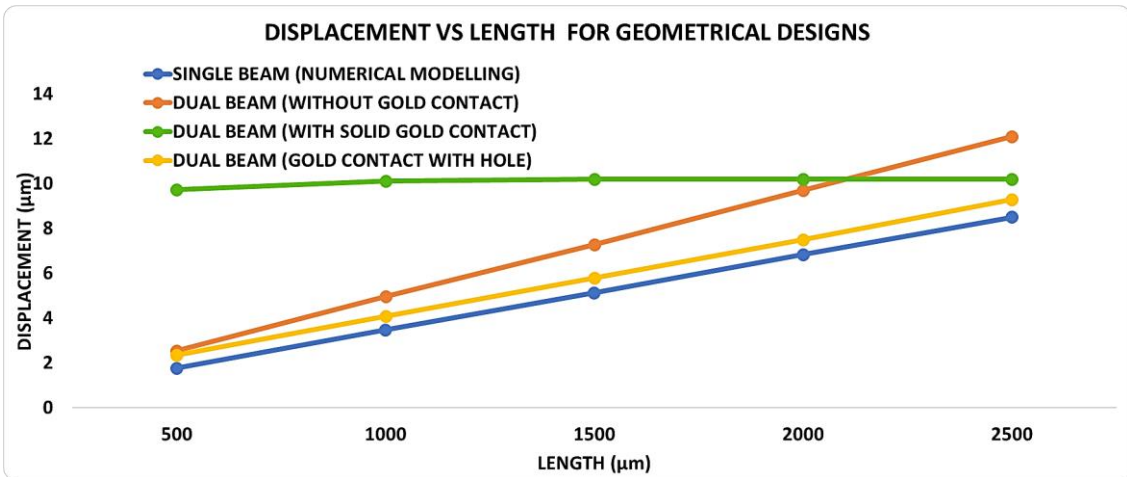


Figure 23. Displacement versus beam length for the four geometries

Figure 22 compares the results obtained from MATLAB to results obtained in COMSOL for single beam design. From Figure 22, it can be observed that the FEM simulation result agrees with the mathematical modelling result, that displacement is an increasing function of beam Length, although there is a slight variation in the results obtained in these two methods. Figure 23. compares displacement trends of the four different geometries under consideration. It is observed in Figure 23. that, as the beam length changes, the dual beams generate greater displacements compared to the single beam. The dual beam without contact generates as much as twice the displacement in single beam, while the dual beam with gold contact demonstrated a fairly constant displacement of about 10 μm across the beam lengths.

#### 4.5.2 Comparative analysis for varying beam width

The relationship between beam displacement and beam width is examined. The width is swept from 100 $\mu\text{m}$  to 500 $\mu\text{m}$ , while all other parameter values remain the same as in Table 5 above. Results obtained for the various beam structures are illustrated in Figures 24 and 25.

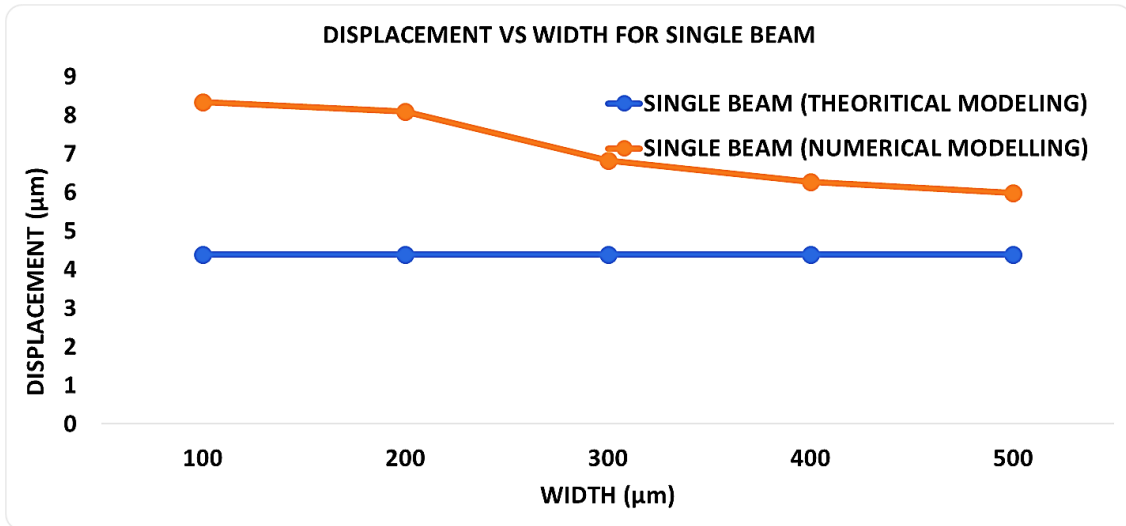


Figure 24. Displacement versus beam width for single beam

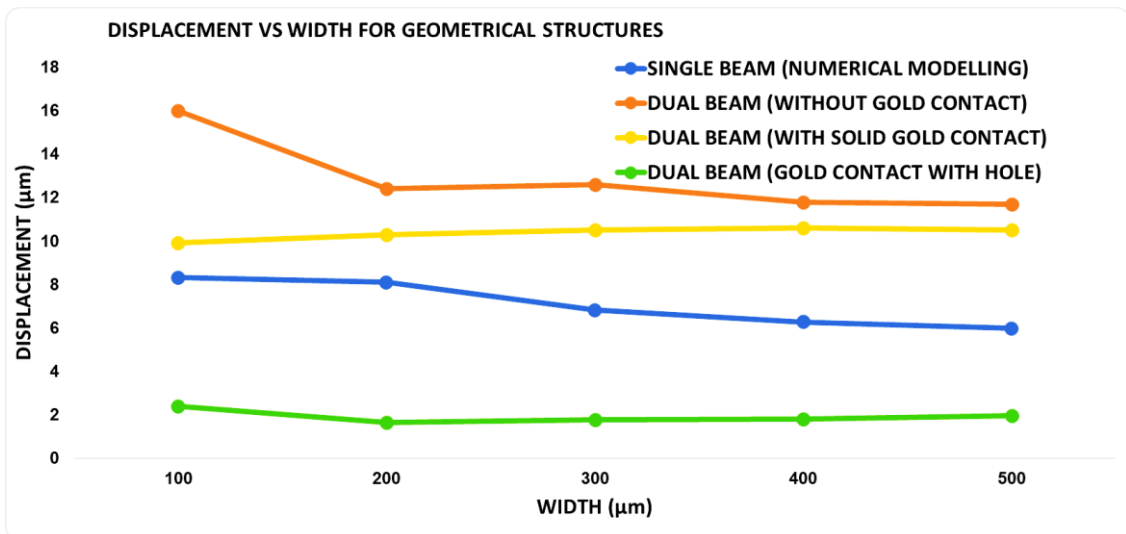


Figure 25. Displacement versus beam width plot for the four geometries

From Figure 24, it is observed that, while the beam displacement obtained in the mathematical model remains flat irrespective of the beam width, the displacement is seen to decrease slightly as the beam width increases in results obtained for FEM analysis. Hence it can be inferred that, when the width is equal for the substrate layer and piezoelectric layer, the displacement slightly changes as the beam width is increased. This

trend is exhibited by all four structures as demonstrated in Figure 25. In addition, Figure 25 demonstrates that the dual beam without gold contact generate almost twice as much displacement as the single beam, followed by the dual beam with perforated gold contact.

#### 4.5.3 Comparative analysis for varying piezoelectric thickness

In this session, the effect of the piezoelectric layer thickness on beam displacement demonstrated by the four different structures for  $t_p$  values between 0.2  $\mu\text{m}$  and 2.5  $\mu\text{m}$  are observed and discussed. All other parameters remain the same as the list in table 2.5. Hence, a beam width of 500  $\mu\text{m}$ , a substrate thickness of 50  $\mu\text{m}$ , beam length of 0.5  $\mu\text{m}$ , and a constant applied voltage of 5V are maintained. The results of this simulation are depicted in Figures 26 and 27.

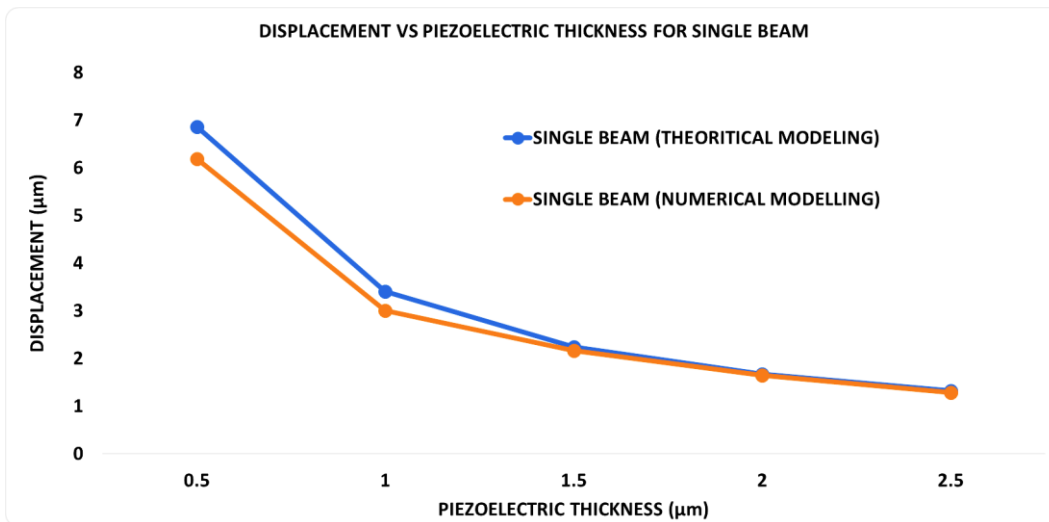


Figure 26. Displacement versus beam piezoelectric thickness for single beam

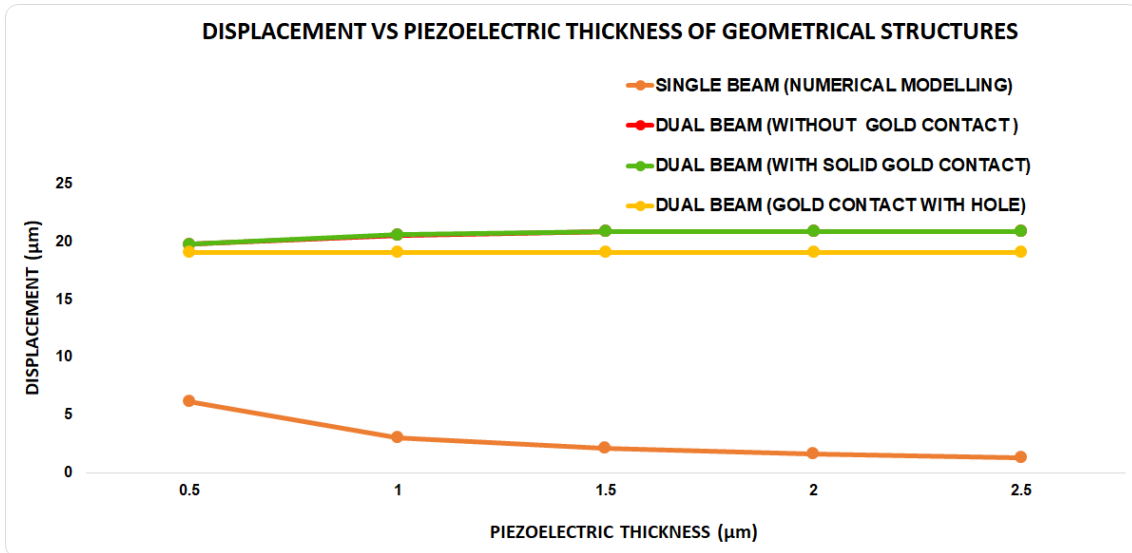


Figure 27. Displacement versus beam piezoelectric thickness for the four geometries

It is observed from Figure 26, that the result from MATLAB agrees with that obtained with COMSOL. Also, it is observed in Figure 27 that the displacements generated by the dual beam structures far exceeds that generated from single beam and were constant as the piezoelectric thickness is varied.

#### 4.5.4 Comparative analysis for varying substrate thickness

Similarly, the effect of varying the substrate thickness on beam displacement for the various geometries is presented and analysed. For this simulation, parameter values used for single beam MATLAB simulations are observed. Hence, beam width of 500 µm, piezoelectric thickness of 0.5 µm, beam length of 0.5 µm, and constant applied voltage of 5V are maintained, while  $t_p$  values between 50 µm and 100 µm are used. Results from MATLAB and COMSOL are compared for a single beam in Figure 28 and results obtained for the four geometries are compared in Figure 29.



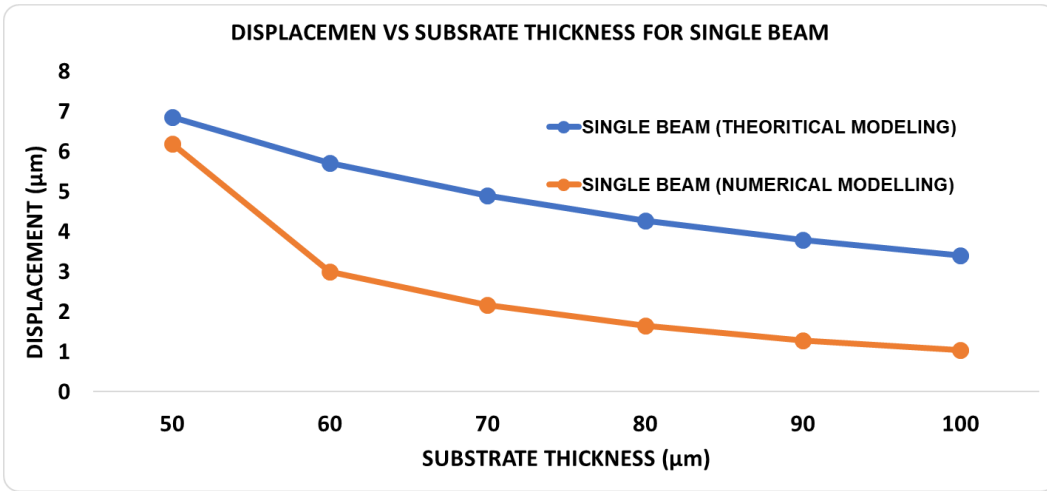


Figure 28. Displacement versus beam substrate thickness for single beam

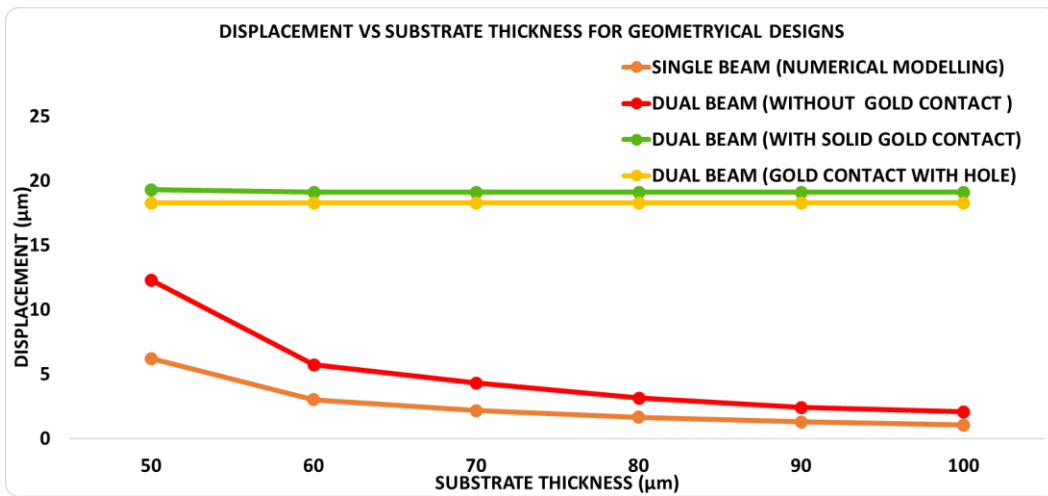


Figure 29. Displacement versus beam substrate thickness plot for the four geometries

From Figure 28, a declining displacement in response to an increase in substrate thickness is observed for a single beam and dual beam without contact. Dual beams with contact exhibit fairly constant displacement as the substrate thickness is increased in Figure 29.

Based on the parametric analysis results above, a summary of the performance of the different geometries in terms of deflection is listed in Table 8. This is done to facilitate the finalization of the optimized geometry which maximizes the deflection for a constant applied voltage to the RF MEMs switch.

Table 7. Comparison of displacement for different geometry at 5V.

Parameter(unit)	Geometry 1 (Single beam)	Geometry 2 (Dual beam without contact)	Geometry 3 (Dual beam with solid Gold contact)	Geometry 4 (Dual beam with perforated gold contact)
Length (500µm-2500µm)	Low	High	Highest	Medium
Width (100µm-500µm)	Medium	Highest	High	Low
Piezoelectric thickness (0.5µm-2.5µm)	Low	High	High	Medium
Substrate thickness (50µm-100µm)	Low	Medium	Highest	High

#### 4.6 Contact force analysis

As previously mentioned, the contact force directly impacts the reliability of the switch. The FEM analysis is conducted to determine the dimension of the switch which provides adequate contact force. Hence a switch geometrical model which provides low actuation voltage while exerting enough contact force is what this analysis seeks to determine.

In COMSOL contact force analysis, the contact surfaces are characterized by 3 main factors:

1. The contact surfaces only touch but do not interpenetrate.
2. They are free to move, separate and move away.
3. They can transmit comprehensive forces.

Similar to the voltage analysis carried out in the previous session, the model of three different geometries are considered to analyse contact force results in COMSOL Figures 30(a-c), illustrate the 3D mode shape results obtained.

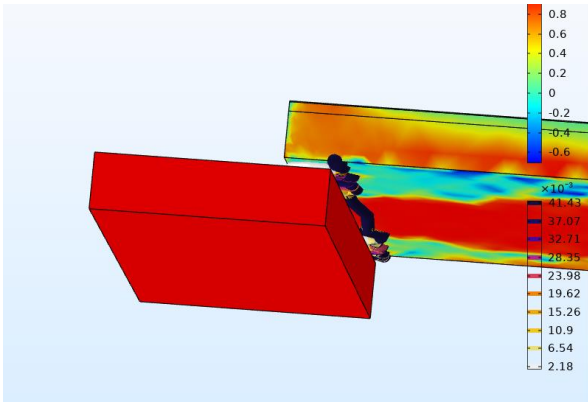


Fig. 30a. Contact pressure for single beam

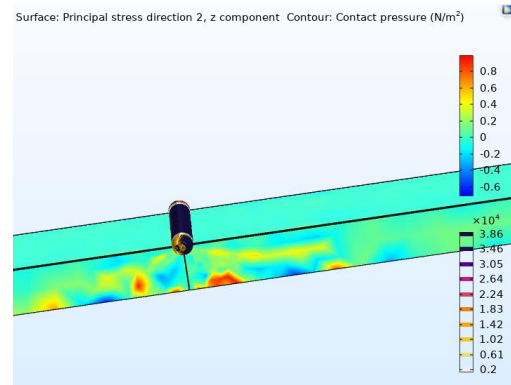


Fig. 30b. Contact pressure for dual beam with solid gold contact

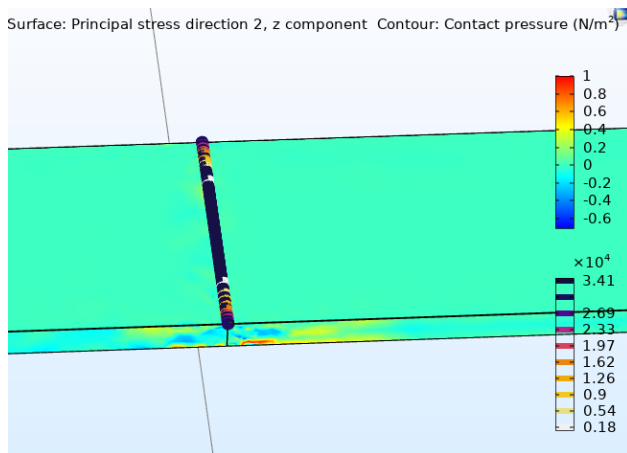


Fig. 30b. Contact pressure for dual beam with gold contact with holes

Figure 30. 3D for contact figure pressure

Figures 30(a-c). represent the 3 D contact pressure plots for the designs under consideration. It can be observed that contact is establish at the contact region in each structure. The optimization results for contact force analysis based on these simulations are presented in the next chapter.

## 4.7 Eigenfrequency analysis

Resonance frequency analysis is carried out in this session. Operating an RF MEMS switch at resonance frequency improves the overall performance of the switch. The natural or resonance frequency depends on many parameters of the switch, particularly the geometry, Young's modulus, and mass of the switch. 3D results obtained from COMSOL modelling are shown in Figures 31(a,b)

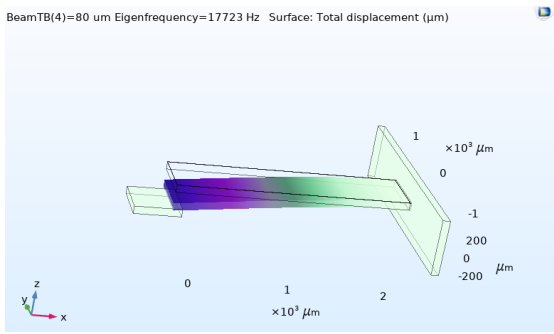


Fig. 31a. Mode shape for single beam

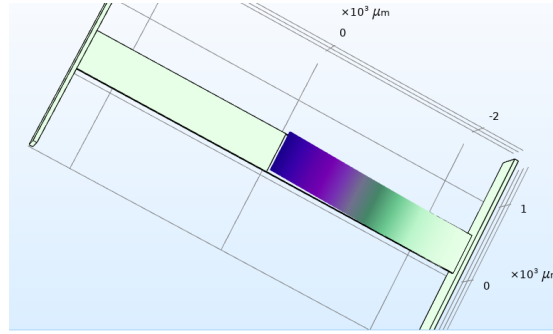


Fig. 31b. Mode shape for dual beams

Figure 31. 3D for eigenfrequency mode shapes

The effect of beam length, width, piezoelectric thickness, substrate thickness, and actuation voltage on the resonance frequency of the four geometries under consideration were studied. By keeping all other variables constant while varying the parameter of interest, the relationship between each parameter and resonance frequency is established.

#### 4.7.1 Comparative analysis for varying beam length

Firstly, the effect of beam length on resonance frequency is examined from Figure 32. It is observed that by increasing the beam length, the resonance frequency reduces. Further it is observed that eigenfrequency in dual beams is about half the eigenfrequency observed in the single beam. All three dual beams exhibit almost equal values of eigenfrequencies across the beam lengths.

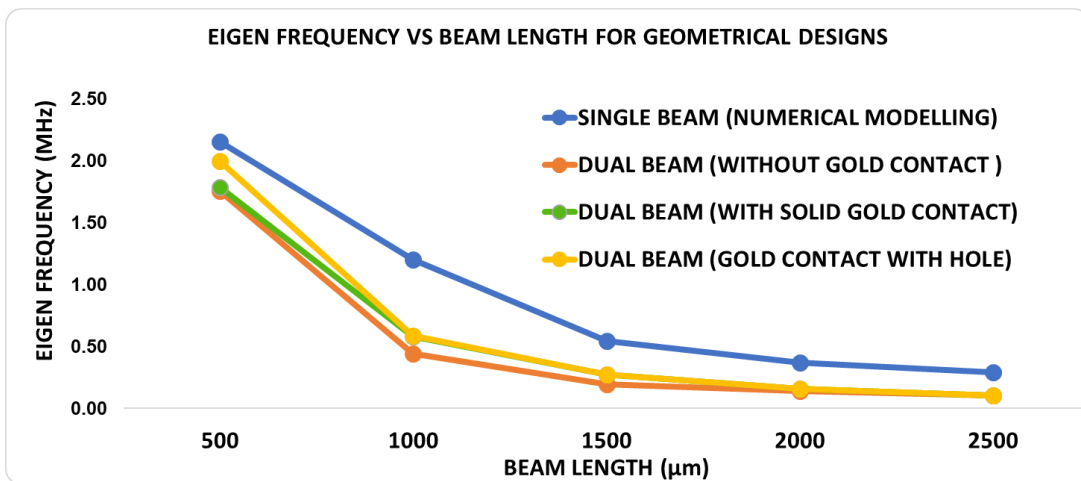


Figure 32. Eigenfrequency versus beam length for the four geometries

### 4.7.2 Comparative analysis for varying beam width

Next, the effect of beam width on resonance frequency is examined from Figure 33., cause From the graph, it can be observed that the resonance frequency of dual beams remains constant from width values 100  $\mu\text{m}$  to 300  $\mu\text{m}$ , and increases slightly at 400  $\mu\text{m}$  and 500  $\mu\text{m}$ . Resonance frequency of single beam increases steadily across the width except at 200  $\mu\text{m}$  where it dips slightly. Overall, it can be inferred from Figure 33. that the effect of changing width on resonance frequency is minimal.

Further is observed that eigenfrequency in dual beams is less than half the eigenfrequency observed in the single beam. All three dual beams exhibit almost equal values of eigenfrequencies across the beam widths.

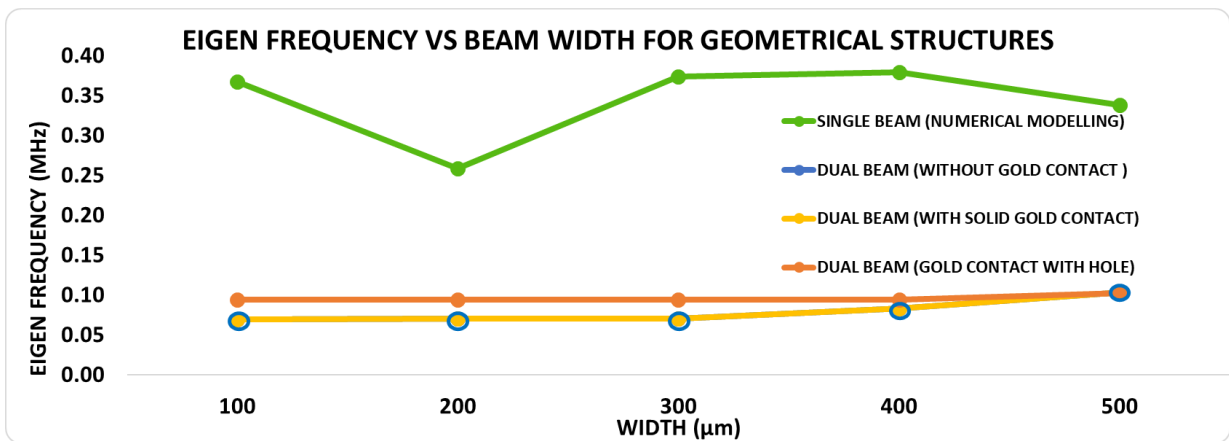


Figure 33. Eigenfrequency versus beam width for the four geometries

### 4.7.3 Comparative analysis for varying substrate thickness

The influence of substrate thickness of beam length is illustrated in Figure 34. In summary, the eigenfrequency of single beam increases linearly as the substrate thickness is increased, while the dual beams have resonance frequencies that remain almost constant irrespective of the substrate value. Here as well, eigenfrequency in dual beams is less than half the eigenfrequency observed in the single beam. All three dual beams exhibit almost equal values of eigenfrequencies across the beam substrate thickness.

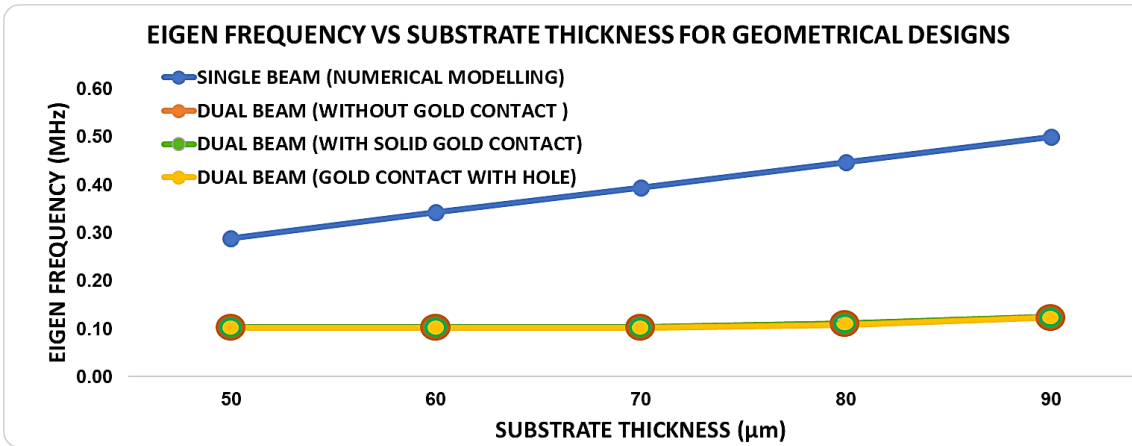


Figure 34. Eigenfrequency versus substrate thickness for the four geometries

#### 4.7.4 Comparative analysis for varying piezoelectric thickness

Similarly, the effect of piezoelectric thickness on eigenfrequency is examined from Figure 35. From this figure, it can be observed the eigenfrequency remains unchanged as the piezoelectric thickness increases. Again, it is observed that eigenfrequency in dual beams is less than half the eigenfrequency observed in the single beam. All three dual beams exhibit almost equal values of eigenfrequencies across the beam piezoelectric thickness.

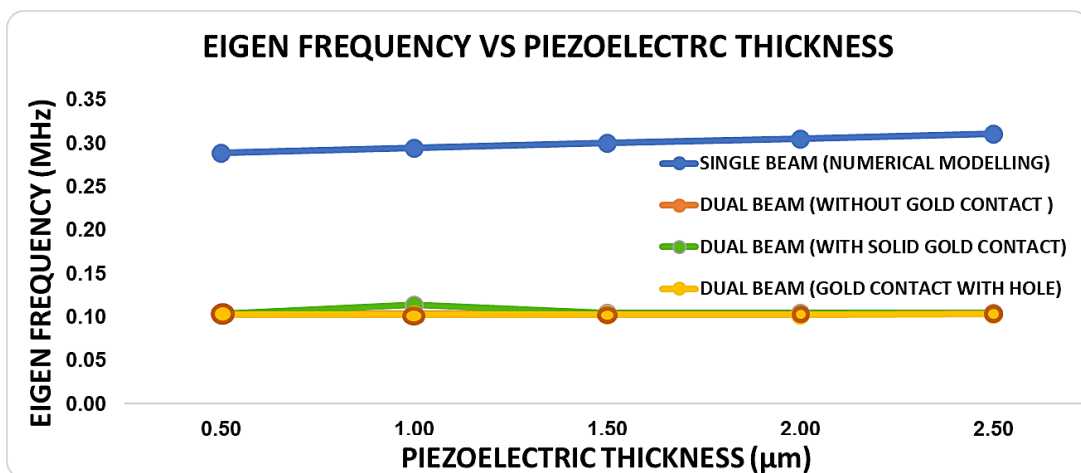


Figure 35. Eigenfrequency versus piezoelectric thickness for the four geometries

#### 4.7.5 Comparative analysis for varying applied voltage

The effect of the applied voltage on eigenfrequency is obtained in Figure 36. The eigenfrequency remains flat as the applied voltage is increased for both single and dual beams. Further the dual beams produce half the eigenfrequency in single beam. In

summary, increasing the thickness, and reducing the length of the beam results in the reduction of the resonance frequency.

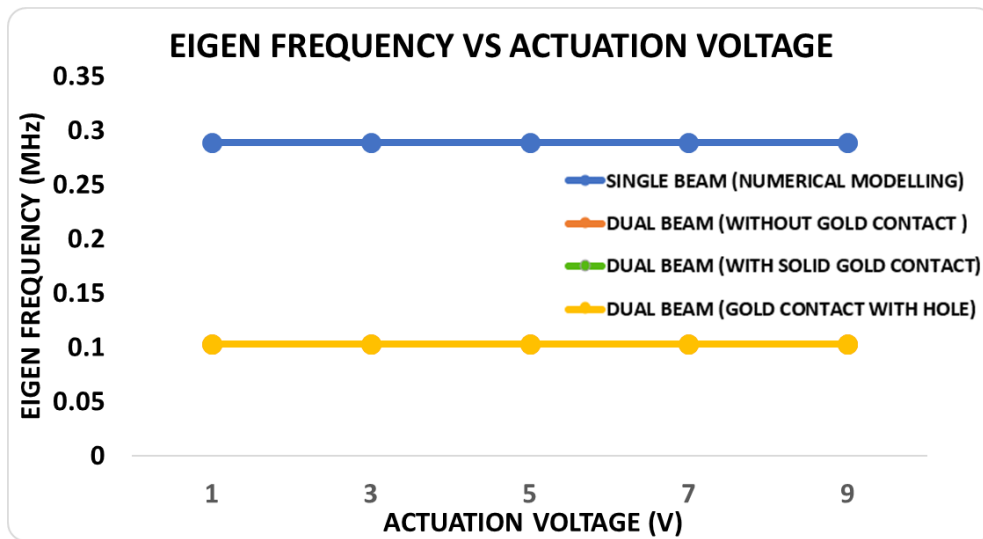


Figure 36. Eigenfrequency versus applied voltage for the four geometries

In summary, the eigenfrequency also depends on the geometry parameter. As such, after concluding in the optimized parameters, the eigenfrequency at which these switch operate will be identified.

## 5 Optimisation

The switch design optimization steps will involve first optimizing one parameter, and then using this parameter as an input for further optimization, to finally obtain all optimized geometry parameters. The desired characteristics of the switch include:

1. Displacement of 10  $\mu\text{m}$  or more at low actuation voltage of 3-5V, for easy integration with CMOS circuitry
2. Linear responds to input voltage.
3. All geometric parameters conform with the fabrication requirements for RF MEMS switches.

First, the length of the beam is optimized. From the parametric studies, the length of the beam is proportional to the beam's displacement. In addition, the actuation voltage required to obtain a desirable displacement decreases as the length increases. Further, the impact of increasing beam length is analysed in Figure 10. From 1000  $\mu\text{m}$  to 2000  $\mu\text{m}$ , the displacement increases by over 100%; from 1500  $\mu\text{m}$  to 2000  $\mu\text{m}$ , the displacement increases by about 70%; from 2000  $\mu\text{m}$  to 2500  $\mu\text{m}$ , the displacement increases by about 50%. Hence, although increasing the length increases the displacement, the impact of this action gradually dwindles. In considering, the negative impact of a relatively long beam on contact force, it is appropriate to select a beam length of 2500  $\mu\text{m}$  as the optimized switch length, and not to exceed this value. This way, limitations imposed by miniaturization, conformity to real-life fabrication requirements, and ability to still obtain high contact force while lowering the actuation voltage can be balanced. It can be observed that, for a single beam, given that all other parameters remain constant, the desirable displacement of 10  $\mu\text{m}$  is achieved at a length of 2500  $\mu\text{m}$  when the actuation voltage of 7V is applied in a single beam, and at a voltage of 5V in 3 all three dual beam geometries.

Next, the substrate thickness is optimised. As opposed to the beam's response to increasing length, the displacement of the beam is observed to be inversely proportional to the thickness of the substrate. Furthermore, a slight modification of the beam thickness plays a key role in the displacement generated, and hence in the actuation voltage required. For instance, a 10% increase in substrate thickness, results in a corresponding 17% average decline in displacement as illustrated in Figure 8. Hence, it would be



recommended to make the substrate as thin as possible. Hence, the optimised substrate thickness selected is 50  $\mu\text{m}$ .

Third, the piezoelectric thickness is optimised. From Figure 7, it is seen that displacement is a decreasing function of  $t_p$ . In addition, the contact force is also a decreasing function of the piezoelectric thickness as shown in Figure 17. Although overall, the impact of decreasing piezoelectric thickness on actuation voltage and contact force, is not as dramatic as for substrate thickness, the impact of increasing the piezoelectric thickness from 0.5  $\mu\text{m}$  to 1  $\mu\text{m}$  on displacement is dramatic. It is beneficial to design the switch with as thin a piezoelectric film as possible, in order to achieve the minimum actuation voltage and maximised contact force. For these reasons, the optimised piezoelectric thickness value is 0.5  $\mu\text{m}$ .

Next, the width of the beam is optimised. As previously mentioned, the piezoelectric layer has the same width as the substrate layer. In both FEM and MATLAB simulations, it is observed in Figure 9. that the impact of the width on displacement and actuation voltage is rather minimal. However, it is observed in Figure 16. that increasing the width considerably increases the contact force. It should also be mentioned that the width of the RF MEMS switch may also be constrained by electrical parameters, such as isolation and insertion loss. Since this scope of work does not include analysis of losses, the optimised width that provides the lowest voltage with a high contact force is 500  $\mu\text{m}$ .

The initial switch gap is also optimized. The switch gap is inversely proportional to the contact force and the actuation voltage. Hence. the minimum practical switch gap value of 500nm is selected.

Finally, in recent times, owing to C-axis orientation, AlN materials can be fabricated with improved piezoelectric coefficient values as high as  $-2.8\text{pm/V}$ .

The cross-sectional dimensions of the optimized design are: Length 2000  $\mu\text{m}$ , Width 500  $\mu\text{m}$ , Substrate thickness 50  $\mu\text{m}$ , piezoelectric thickness 0.5  $\mu\text{m}$ , switch gap 500nm, and AlN piezoelectric coefficient of  $-2.8\text{pm/V}$ . Using these parameters for the switch design, actuation voltage of 7V for a single beam and 5V for the dual beams as shown in Figure 37 and Figure 38.

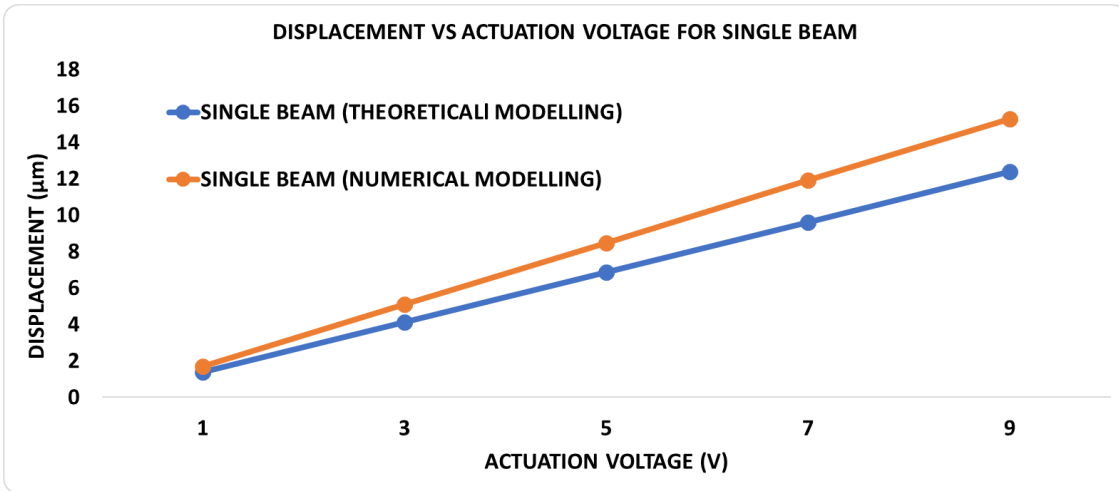


Figure 37. Displacement versus voltage for optimized geometry (Single Beam)

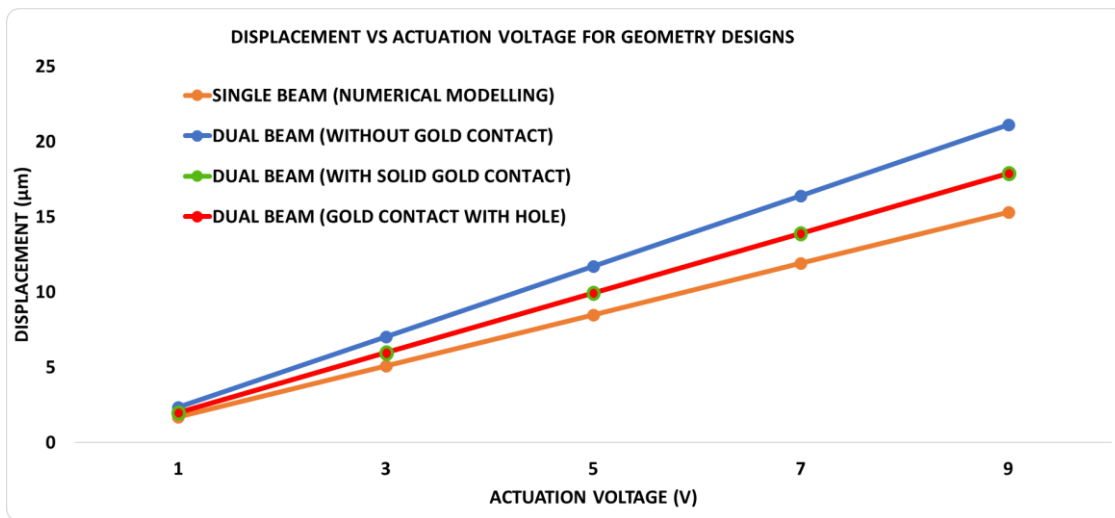


Figure 38. Displacement versus voltage for optimized geometry (All four geometries)

From Figure 36. It is observed that, at 7V, displacement of 10 µm is achieved for single beam. Figure 37 shows that, at any given voltage, the displacements attained by dual beams are greater compared to single beam. While dual beams with gold contacts (solid contact and perforated-edge contact) generate the same displacements across the varying voltages, the maximum displacement values are observed in dual beam with gold contact.

Using the optimized geometry parameters, contact force of 0.0015µN and 0.2µN are obtained at constant voltage of 5V. Figures 39 and 40, show how the contact force of the optimized geometry changes with increase in voltage.

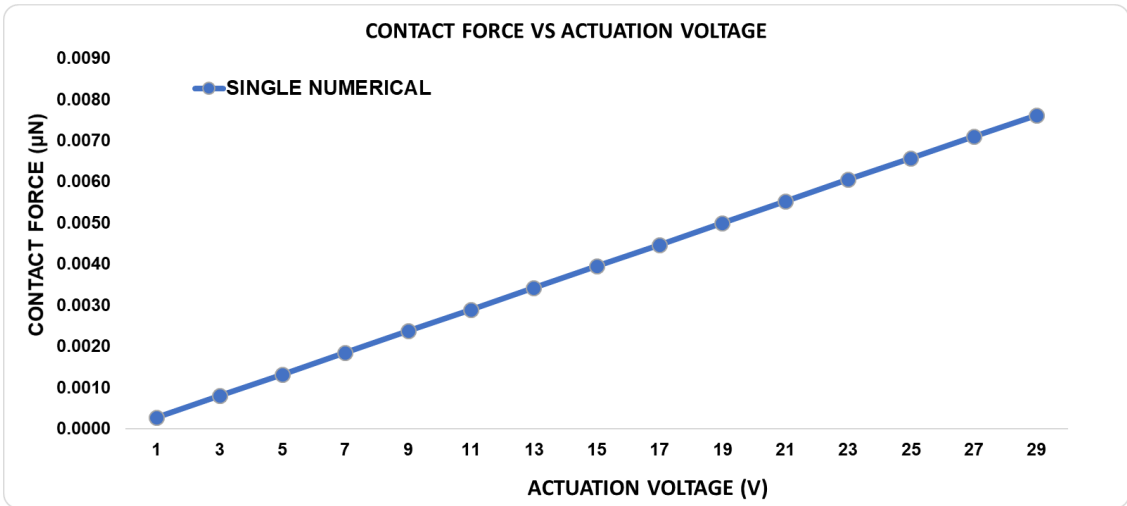


Figure 39. Contact force vs actuation voltage for single beam

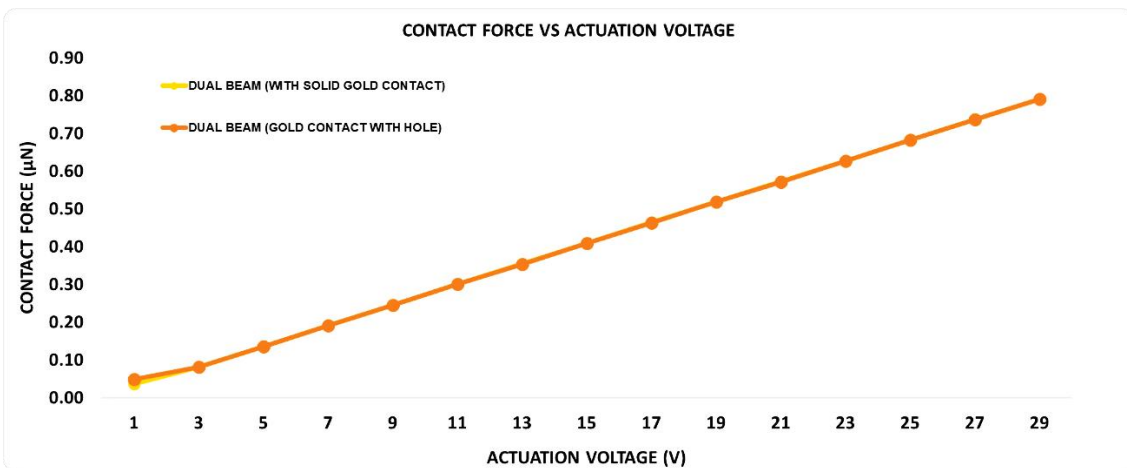


Figure 40. Contact force vs actuation voltage for dual beams with contact

Finally, using the optimised geometrical parameters, the single beam and dual beam RF MEMS switches show resonance frequencies are 3.5MHz and 1.32MHz respectively.

## 6 Summary

In this work, four geometrical structures were designed. Piezoelectric actuation mechanism was employed for obtaining low actuation voltage and high contact force. Parametric analysis involving geometry cross-sectional dimensions and material properties were undertaken to achieve optimized designs. The optimized switch design dimensions obtained are length 2500  $\mu\text{m}$ , width 500  $\mu\text{m}$ , substrate thickness 50  $\mu\text{m}$ , piezoelectric thickness 0.5  $\mu\text{m}$ , switch gap 500nm, and AlN piezoelectric coefficient of -2.8pm/V. Using the optimized parameters, the single beam and dual beams provide actuation voltage of 7V and 5V respectively. Consequently, at any given constant voltage, the dual beam generated almost twice the displacement of the single beam. From the optimization analysis, contact force of 0.009 $\mu\text{N}$  in the single beam and 0.9 $\mu\text{N}$  in dual beam are achieved. Furthermore, the single beam and dual beam RF MEMS switches show resonance frequencies are 3.5MHz and 1.32MHz respectively.

## References

- [1] Yadav, R., Yadav, R., Nehra V and Rangara K J 2011 RF MEMS Switches: Fabrication, Key Features, Application & Design Tools **3** 179–83
- [2] Ashish Kumar Sharma, “Design, Simulation and Analysis of RF- MEMS Switches for Reconfigurable Antennas”, Birla Institute of Technology and Science, Pilani 2014
- [3] Mehadi Hasan Ziko and Ants Koel 2018 IOP Conf. Ser.: Mater. Sci. Eng. 362 012002
- [4] G. M. Rebeiz: RF MEMS Switches: Status of The Technology, 1st Edition, John Wiley & Sons, Inc., 2003
- [5] Gabriel M. Rebeiz, RF MEMS: THEORY, DESIGN, AND TECHNOLOGY, Wiley, January 2003. DOI:10.1002/0471225282
- [6] Cho, I. J., Song, T., Back, S. H., & Yoon, E. (2004). A low-voltage and low-power RF MEMS switch actuated by combination of electromagnetic and electrostatic forces. In Conference Proceedings- 34th European Microwave Conference (pp. 1445-1448). (Conference Proceedings- European Microwave Conference; Vol. 3).
- [7] Ikehashi, T. & Ogawa, E. & Yamazaki, H. & Ohguro, Tatsuya. (2007). A 3V Operation RF MEMS Variable Capacitor using Piezoelectric and Electrostatic Actuation with Lithographical Bending Control. 149-152. 10.1109/SENSOR.2007.4300093.
- [8] D. Saias, P. Robert, S. Boret, C. Billard, G. Bouche, D. Belot, and P. Ancey, “An above IC MEMS RF switch,” IEEE J. Solid-State Circuits 38(12), 2318–2324 (2003). DOI: 10.1109/JSSC.2003.819170
- [9] Sravani, Girija & Karumuri, Srinivasa Rao. (2017). Analysis of RF MEMS shunt capacitive switch with uniform and non-uniform meanders. Microsystem Technologies. 10.1007/s00542-017-3507-5
- [10] Tian W, Li P, Yuan L. Research and Analysis of MEMS Switches in Different Frequency Bands. Micromachines (Basel). 2018;9(4):185. Published 2018 Apr 15. doi:10.3390/mi9040185
- [11] Yole Développement. ‘RF-MEMS: From Technology Push to Market Pull’. [ONLINE], Available at: <http://www.microwave-rf.com/docs/10h15-Yole.pdf> [Accessed 10 October 2019]
- [12] Yole Développement. ‘Status of the MEMS Industry report’ – [ONLINE], Available at: [http://www.yole.fr/MEMSManufacturers\\_Ranking\\_2016.aspx#.XhhypUczY2M](http://www.yole.fr/MEMSManufacturers_Ranking_2016.aspx#.XhhypUczY2M) [Accessed 9 November 2019]
- [13] EETAsia ‘The curious case of the maturing MEMS market’– [ONLINE], Available at: [https://archive.eetasia.com/www.eetasia.com/ART\\_8800717597\\_480500\\_NT\\_9fe17084.HTM](https://archive.eetasia.com/www.eetasia.com/ART_8800717597_480500_NT_9fe17084.HTM) [Accessed 9 November 2019]
- [14] MarketWatch. ‘Global Radio Frequency (RF) MEMS Market 2019-2023’. [ONLINE] Available <https://www.marketwatch.com/press-release/global-radio-frequency-rf-mems-market-2019-2023-expected-to-grow-at-a-cagr-of-approx-37-with-aac-technologies-analog-devices-broadcom-cavendish-kinetics-and-qorvo-at-the-forefront---researchandmarketscFBARom-2019-02-21> [Accessed 09 September 2019]
- [15] Fraga, Mariana & Furlan, Humber & Pessoa, Rodrigo & Massi, Marcos. (2013). Wide bandgap semiconductor thin films for piezoelectric and piezoresistive MEMS sensors applied at high temperatures: An overview. Microsystem Technologies. 20.9-21. 10.1007/s00542-013-2029-z.

- [16] Khan A, Abas Z, Soo Kim H and Oh I K 2016 Piezoelectric thin films: An integrated review of transducers and energy harvesting *Smart Mater. Struct.* 25. DOI: 10.1088/0964-1726/25/5/053002
- [17] M. Manivannan, R. Joseph Daniel, and K. Sumangala, "Low Actuation Voltage RF MEMS Switch Using Varying Section Composite Fixed-Fixed Beam," *International Journal of Microwave Science and Technology*, vol. 2014, Article ID 862649, 12 pages, 2014. <https://doi.org/10.1155/2014/862649>.
- [18] Li Ya, Ma & Soin, Norhayati & Daut, Mohamad & Hatta, Sharifah. (2019). Comprehensive Study on RF MEMS Switches Used for 5G Scenario. *IEEE Access*. 7. 1-1. 10.1109/ACCESS.2019.2932800.
- [19] Klaasse, G. & Puers, Robert & Tilmans, H.A.C. (2003). Piezoelectric Versus Electrostatic Actuation for a Capacitive RF MEMS Switch
- [20] Li, Hao & Ruan, Yong & You, Zheng & Song, Zhiqiang. (2020). Design and Fabrication of a Novel MEMS Relay with Low Actuation Voltage. *Micromachines*. 11. 171. 10.3390/mi11020171.
- [21] Zhang M, Yang J, Si C, Han G, Zhao Y and Ning J 2015 Research on the piezoelectric properties of AlN thin films for MEMS applications *Micromachines* 6 1236–48 doi:10.3390/mi6091236
- [22] Lee, Hee & Park, Jae-Yeong & Lee, Kyeong-Hak & Nam, Hyo-Jin & Bu, Jong. (2004). Silicon bulk micromachined RF MEMS switches with 3.5 volts operation by using piezoelectric actuator. 2. 585 - 588 Vol.2. 10.1109/MWSYM.2004.1336049.
- [23] Lee, Hee & Park, Jae-Yeong & Bu, Jong-Uk. (2005). Piezoelectrically actuated RF MEMS DC contact switches with low voltage operation. *Microwave and Wireless Components Letters, IEEE*. 15. 202 - 204. 10.1109/LMWC.2005.845689.
- [24] Polcawich, Ronald & Pulskamp, Jeffrey & Judy, Daniel & Ranade, Prashant & Trolier-McKinstry, S. & Dubey, Madan. (2008). Surface Micromachined Microelectromechanical Ohmic Series Switch Using Thin-Film Piezoelectric Actuators. *Microwave Theory and Techniques, IEEE Transactions on*. 55. 2642 - 2654. 10.1109/TMTT.2007.910072.
- [25] Polcawich, R. G., Judy, D., Pulskamp, J. S., Trolier-McKinstry, S., & Dubey, M. (2007). Advances in piezoelectrically actuated RF MEMS switches and phase shifters. In 2007 IEEE MTT-S International Microwave Symposium Digest (pp. 2083-2086). [4264279] (IEEE MTT-S International Microwave Symposium Digest). doi:10.1109/MWSYM.2007.380297
- [26] Guerre, Roland & Drechsler, Ute & Bhattacharyya, Debabrata & Rantakari, Pekka & Stutz, Richanne & Wright, Robert & Milosavljevic, Zlatoljub & Vaha-Heikkila, Tauno & Kirby, Paul & Despont, M. (2010). Wafer-level transfer technologies for PZT-based RF MEMS switches. *Microelectromechanical Systems, Journal of*. 19. 548 - 560. 10.1109/JMEMS.2010.2047005.
- [27] Nakatani, Takayoshi, T. Katsuki, Hisao Okuda, Osamu Toyoda, S. Ueda and Fumihiko Nakazawa. "PZT-actuated reliable RF MEMS switch using single-crystal silicon asymmetric beam." *Asia-Pacific Microwave Conference 2011* (2011): 554-557.
- [28] Ivanov, Tony G. et al. "Shunt RF MEMS contact switch based on PZT-on-SOI technology." *2012 IEEE/MTT-S International Microwave Symposium Digest* (2012): 1-3.
- [29] Nakatani, T., Katsuki, T., Okuda, H., Toyoda, O., Ueda, S., & Nakazawa, F. (2011). PZT-actuated reliable RF MEMS switch using single-crystal silicon asymmetric beam. *Asia-Pacific Microwave Conference 2011*, 554-557.

- [30] Giffney, T., Aw, K., Yu, M. et al. Design and modeling of a continuously variable piezoelectric RF MEMS switch. *Microsyst Technol* 21, 1293–1300 (2015). <https://doi.org/10.1007/s00542-014-2168-x>
- [31] Yu, H.W., Kim, J. Low-voltage micromechanical RF switch based on a piezoelectric micro-cantilever integrated with a transmission line. *Journal of the Korean Physical Society* 67, 1942–1946 (2015). <https://doi.org/10.3938/jkps.67.1942>
- [32] Mahameed, Rashed & Sinha, Nipun & Pisani, Marcelo & Piazza, Gianluca. (2008). Dual-Beam Actuation of Piezoelectric AlN RF MEMS Switches Monolithically Integrated with AlN Contour-Mode Resonators. *Journal of Micromechanics and Microengineering - J MICROMECHANIC MICROENGINEER*. 18. 10.1088/0960-1317/18/10/105011.
- [33] N. Sinha, R. Mahameed, C. Zuo and G. Piazza, "Integration of AlN micromechanical contour-mode technology filters with three-finger dual beam AlN MEMS switches," 2009 IEEE International Frequency Control Symposium Joint with the 22nd European Frequency and Time forum, Besancon, 2009, pp. 1-4. doi: 10.1109/FREQ.2009.5168131
- [34] P.C.Tembhare et al, AlN RF MEMS switches for low actuation voltage . 24. 10.5755/j01.eie.24.5.2167542.
- [35] Lim, Yang Choon & Kouzani, Abbas & Duan, Wei & Kaynak, Akif. (2010). Effects of design parameters on sensitivity of microcantilever biosensors. 2010 IEEE/ICME International Conference on Complex Medical Engineering, CME2010. 177 - 181. 10.1109/ICCME.2010.5558847.
- [36] Lim, C.W., Wang, C.M. & Kitipornchai, S. Timoshenko curved beam bending solutions in terms of Euler-Bernoulli solutions. *Arch. Appl. Mech.* 67, 179–190 (1997). <https://doi.org/10.1007/s004190050110>
- [37] Mintz I (2007), Euler-Bernoulli beam theory - each section is at 90deg to the axis. [Accessed 23/04/20] [https://commons.wikimedia.org/wiki/File:Euler-Bernoulli\\_beam\\_theory.png](https://commons.wikimedia.org/wiki/File:Euler-Bernoulli_beam_theory.png)
- [38] Chen, X. & Fox, C. & McWilliam, Stewart. (2004). Optimization of a Cantilever Microswitch with Piezoelectric Actuation. *Journal of Intelligent Material Systems and Structures - J INTEL MAT SYST STRUCT*. 15. 823-834. 10.1177/1045389X04044128.
- [39] Hwang, Woo & Park, Hyun. (1993). Finite element modeling of piezoelectric sensors and actuators. *Aiaa Journal - AIAA J*. 31. 930-937. 10.2514/3.11707.
- [40] Wellman Brush, WB, (2009), Importance of Contact Force, [online] Available at <https://materion.com/-/media/files/alloy/newsletters/technical-tidbits/issue-no-06---the-importance-of-contact-force.pdf> [Accessed 23/04/20]]
- [41] Mulloni, Viviana & Iannacci, Jacopo & Bartali, Ruben & Victor, Micheli & Colpo, Sabrina & Laidani, Nadhira & Margesin, Benno. (2012). Gold-based thin multilayers for ohmic contacts in RF MEMS switches. *Microsystem Technologies*. 18. 10.1007/s00542-011-1421-9.
- [42] Nath, V. Springer book on Proceedings of the International Conference on Nano-electronics, Circuits & Communication Systems Mar 24, 2017 - Technology & Engineering